Targeting PPARα/γ by icariside II to rescue acute liver injury via coactivating SIRT6

Jianmei Gao[1], Jiajia Wei[1], Yang Yi[1], Miaoxian Gong[1], Fangqin Hou[1], Xiaoyu Wu[1], Yiqi Li[1], Yuandong Zhang[1], and Qihai Gong[1]

[1]Zunyi Medical University

April 05, 2024

Abstract

Background and Purpose:: Peroxisome proliferator-activated receptor α and-γ (PPARα/γ) are known to play crucial roles in acute liver injury (ALI). Icariside II (ICS II), a natural flavonoid compound derived from Herba Epimedii, confers neuroprotection with PPARα/γ induction potency. This study was aimed to explore whether ICS II has the capacity to protect against ALI, and if so what are the role of PPARα/γ in the beneficial effect of ICS II on ALI. Experimental Approach: Mice challenged by D-galactosamine (GalN)/lipopolysaccharide (LPS) and Kupffer cells (KCs) upon LPS insult were used as ALI models in vivo and in vitro. PPARα/γ-deficient mice and Sirt6-deficient mice were treated with ICS II to validate the potential targets of ICS II on ALI. Key results: ICS II dose-dependently improved the survival rate and liver histology, decreased ALT and AST in D-galactosamine (GalN)/lipopolysaccharide (LPS)-treated mice. Furthermore, ICS II directly bound to PPARα/γ and increased their activities. The protective properties of ICS II were counteracted when PPARα/γ were knocked out in GalN/LPS-induced mice and LPS-induced KCs, respectively. Mechanistically, ICS II restored mitochondrial function, reduced oxidative stress and inflammation through activating PPARα/γ, which interacted with Sirt6 and inhibited NF-κB nuclear translocation. Intriguingly, ICS II-evoked hepatoprotective effect and activation of PPARα/γ were largely blunted in Sirt6-deficient mice. Conclusions and implications: Our findings not only highlight PPARα/γ-SIRT6 signaling as a vital therapeutic target to combat ALI, but also reveal ICS II may serve as a novel dual PPARα/γ agonist to safeguard ALI from the oxidation-inflammation vicious circle by coactivating SIRT6.

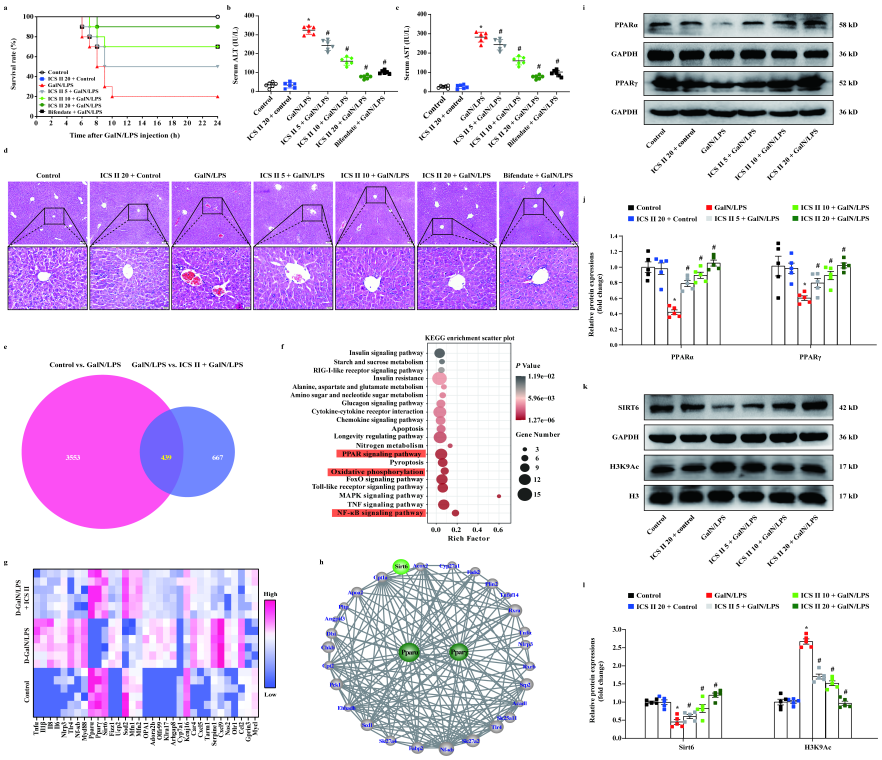

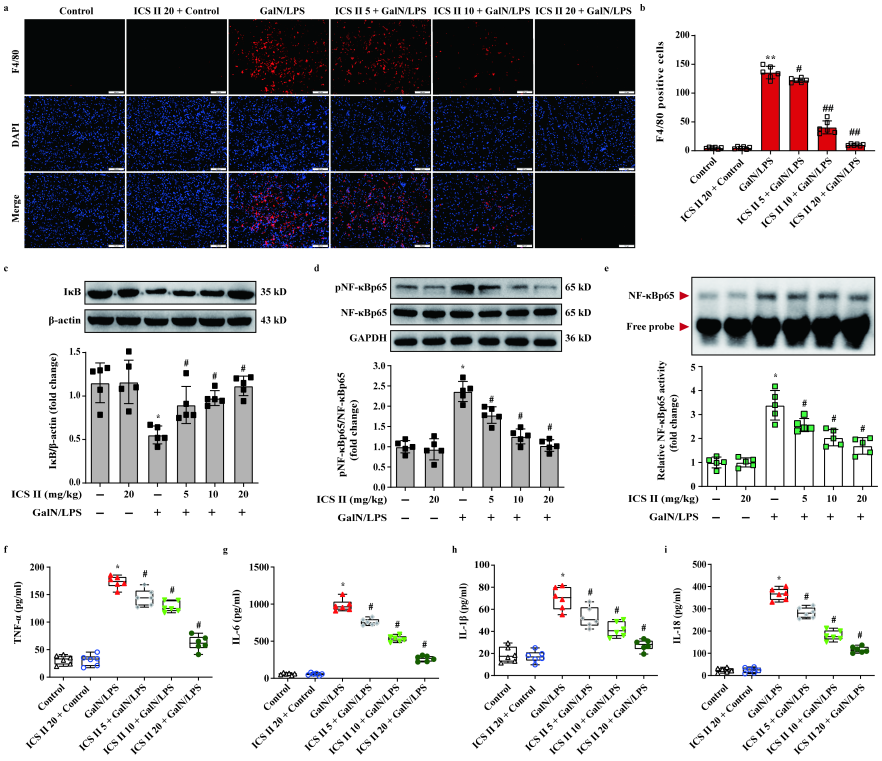

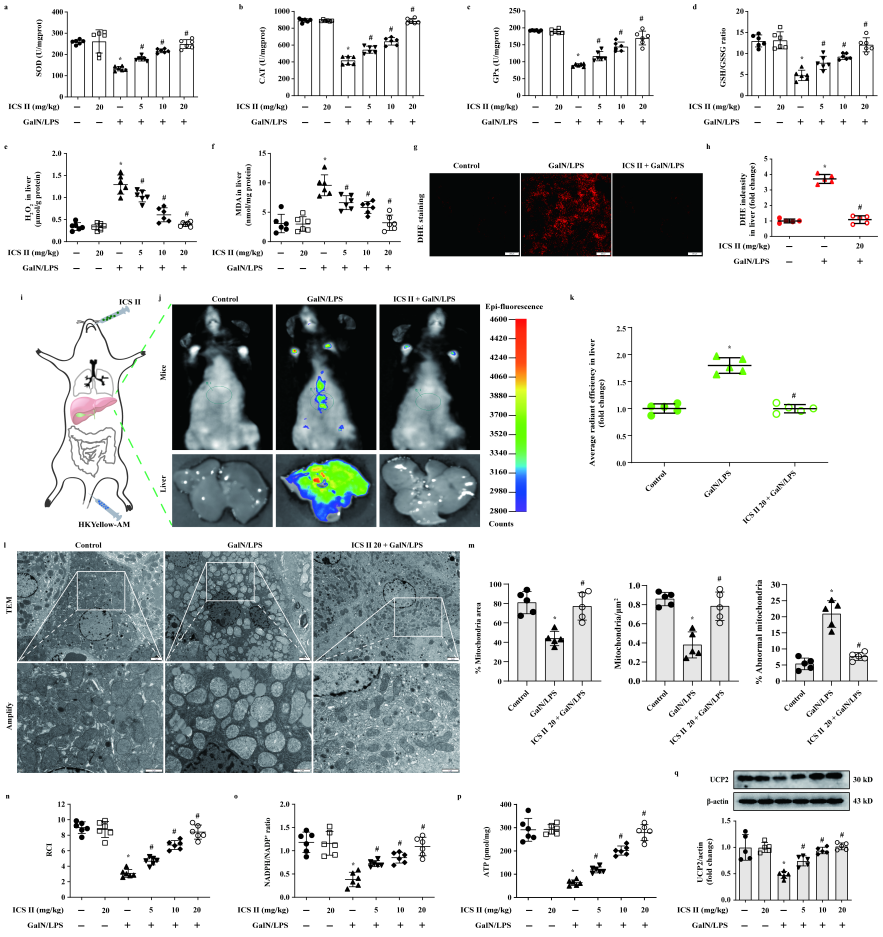

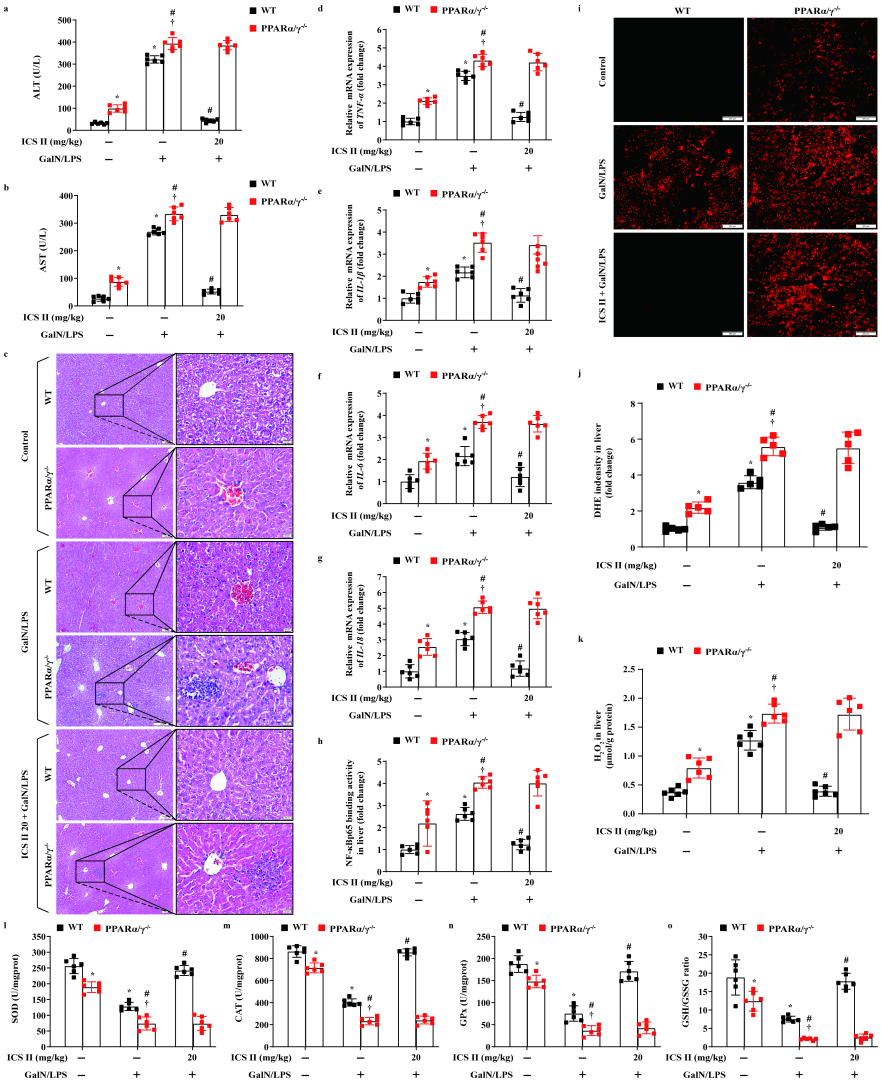

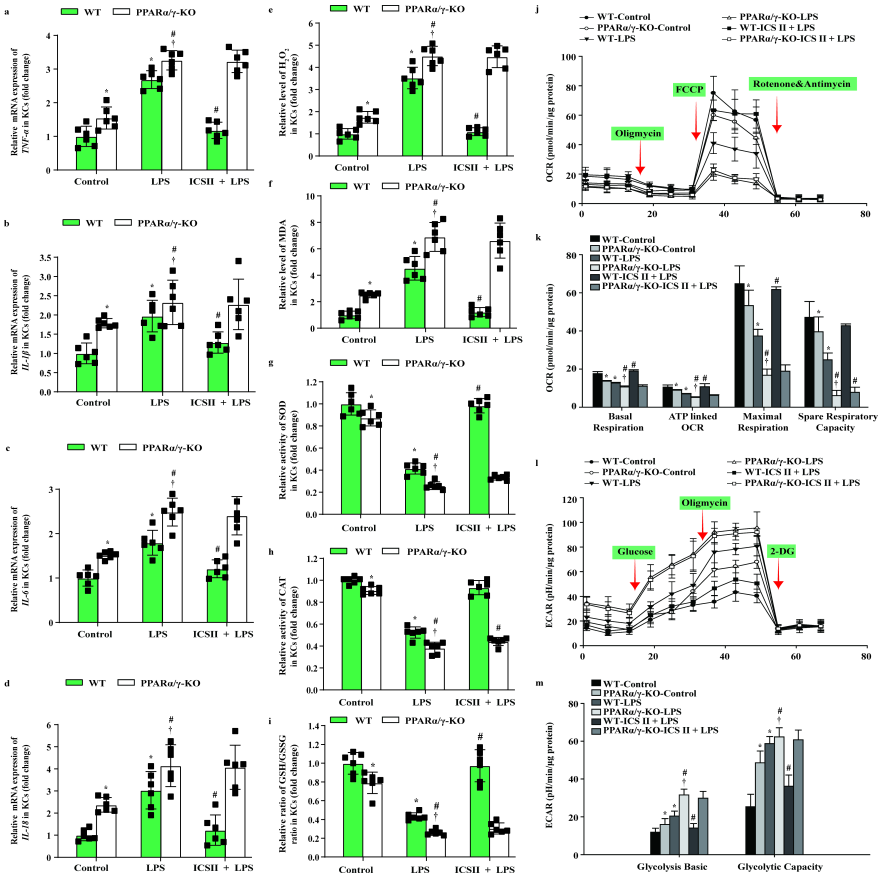

Targeting PPARα/γ by icariside II to rescue acute liver injury *via* coactivating SIRT6

Jianmei Gao[1,2,3], Jiajia Wei[1,2], Yang Yi[1,2,3], Miaoxian Gong[1,2,3], Fangqin Hou[1,2,3], Xiaoyu Wu[1,2.3], Yiqi Li[1,2.3], Yuandong Zhang[1,2.3], Qihai Gong[1,2,3*]

[1]Key Laboratory of Basic Pharmacology of Ministry of Education and Joint International Research Laboratory of Ethnomedicine of Ministry of Education, Zunyi Medical University, Zunyi, China

[2]Department of Pharmacology, Key Laboratory of Basic Pharmacology of Guizhou Province and School of Pharmacy, Zunyi Medical University, Zunyi, Guizhou, China

[3]Chinese Pharmacological Society-Guizhou Province Joint Laboratory for Pharmacology, Zunyi Medical University, Zunyi, Guizhou, China

*Corresponding author: Prof. Qihai Gong, Ph.D.

6 Xuefu West Road, Zunyi City, Guizhou Province, 563000, P. R. China

Tel: +86-851-286-423-03

Fax: +86-851-286-423-03

E-mail: gqh@zmu.edu.cn

Acknowledgements

This work was supported by Natural Science Foundation of China (No. 82260781), The ‘‘hundred’’ level of high-level innovative talents in Guizhou Province (No. GCC[2023]042), The future ‘techelite’ talent development program from Zunyi Medical University (No. ZYSE-2020-02), Science and technology planning project of Zunyi (No. ZKHHZ[2022]412), Scientific Research Fund of Graduate of Zunyi Medical University (No. ZYK191), 2011 Collaborative Innovation Center of Traditional Chinese Medicine in Guizhou Province (No. [2022]026).

Author contributions

QHG was responsible for the conception and design of this manuscript. JMG, YY, JJ W, MXG, XYW, FQH and YDZ were responsible for the experiments, acquisition of data and statistical analysis. JMG was responsible for drafting of the manuscript. Approval of the final version of the manuscript on behalf of all authors was done by QHG.

Conflict of interest

The authors declare no conflict of interest.

Declaration of transparency and scientific rigour

This Declaration acknowledges that this paper adheres to the principles for transparent reporting and scientific rigour of preclinical research as stated in the BJP guidelines for Design & Analysis, Immunoblotting and Immunochemistry and Animal Experimentation and as recommended by funding agencies, publishers and other organizations engaged with supporting research.

Abstract

Background and Purpose: Peroxisome proliferator-activated receptor α and-γ (PPARα/γ) are known to play crucial roles in acute liver injury (ALI). Icariside II (ICS II), a natural flavonoid compound derived from *Herba Epimedii*, confers neuroprotection with PPARα/γ induction potency. This study was aimed to explore whether ICS II has the capacity to protect against ALI, and if so what are the role of PPARα/γ in the beneficial effect of ICS II on ALI.

Experimental Approach: Mice challenged by D-galactosamine (GalN)/lipopolysaccharide (LPS) and Kupffer cells (KCs) upon LPS insult were used as ALI models *in vivo* and *in vitro*. PPARα/γ-deficient mice and Sirt6-deficient mice were treated with ICS II to validate the potential targets of ICS II on ALI.

Key results: ICS II dose-dependently improved the survival rate and liver histology, decreased ALT and AST in D-galactosamine (GalN)/lipopolysaccharide (LPS)-treated mice. Furthermore, ICS II directly bound to PPARα/γ and increased their activities. The protective properties of ICS II were counteracted when PPARα/γ were knocked out in GalN/LPS-induced mice and LPS-induced KCs, respectively. Mechanistically, ICS II restored mitochondrial function, reduced oxidative stress and inflammation through activating PPARα/γ, which interacted with Sirt6 and inhibited NF-κB nuclear translocation. Intriguingly, ICS II-evoked hepatoprotective effect and activation of PPARα/γ were largely blunted in Sirt6-deficient mice.

Conclusions and implications: Our findings not only highlight PPARα/γ-SIRT6 signaling as a vital therapeutic target to combat ALI, but also reveal ICS II may serve

as a novel dual PPARα/γ agonist to safeguard ALI from the oxidation-inflammation vicious circle by coactivating SIRT6.

Keywords: acute liver injury; icariside II; PPARα; PPARγ; SIRT6; NF-κB

Bullet point summary

What is already known

• The oxidation-inflammation vicious circle promotes acute liver injury *via* PPARα/γ-SIRT6 signaling.

• Icariside II (ICS II), a natural flavonoid compound derived from *Herba Epimedii*, confers neuroprotection with anti-inflammatory and anti-oxidant effects.

What this study adds

• Icariside II rescues acute liver injury by inhibiting the oxidation-inflammation vicious circle.

• Icariside II is identified as a natural-occurring PPARα/γ-modulating ligand.

• Icariside II promotes PPARα/γ expressions to safeguard acute liver injury by coactivating SIRT6.

What is the clinical significance

• Icariside II as a novel potential PPARα/γ dual agonist to combat ALI with a good safety profile.

1. Introduction

Acute liver injury (ALI) is a fatal clinical syndrome induced by sudden and grievous damage to the liver with high mortality and poor prognosis(Xu et al., 2022). ALI is usually caused by viral and bacterial infection, alcohol abuse and hepatotoxic

medications, which result in loss of hepatocytes and liver function and even death(Zhao et al., 2017). Although liver transplantation is the only life-saving treatment option, donor unavailability and serious complications remain challenges and limitations for clinical application of liver transplantation(Chowdhury, Nabila, Adelusi Temitope & Wang, 2020; Kolodziejczyk et al., 2020). Since effective therapeutic tactics for ALI are still not available, the development of a new effective and safe hepatoprotective agent is an urgent clinical need.

The oxidation-inflammation vicious circle plays a crucial role in the pathogenesis of ALI(Gehrke et al., 2018). Under normal conditions, time-limited oxidative stress and inflammation are deemed beneficial to maintain hepatic homeostasis. Yet, excessive and uncontrolled inflammation and oxidative stress result in extensive loss of hepatocytes(Garate-Rascon et al., 2021; Malireddi et al., 2020). Inhibition of hepatic the oxidation-inflammation vicious circle is therefore the potential therapeutic strategy to protect hepatocytes from ALI. Notably, peroxisome proliferator-activated receptors (PPARs) are nuclear receptors whose activation exert cell defense through anti-antioxidant and inflammatory effects(Wang et al., 2022). Three major isoforms of PPARs have been identified as PPARα, PPARβ/δ and PPARγ that are involved in many physiological and pathological processes(Krishna et al., 2021). PPARα/γ have been implicated in hepatic metabolism by its ability to modulate key metabolic players such as SIRT6, one of the sirtuins, function as a histone H3-lysine 9 (H3K9) deacetylase(Zuo et al., 2019). Emerging evidence demonstrates that sirtuins modulate multiple cellular processes associated with antioxidant and redox signaling. Sirtuins

are NAD^+-dependent deacetylases and there are seven sirtuins in mammals (SIRT1-7)(Singh, Chhabra, Ndiaye, Garcia-Peterson, Mack & Ahmad, 2018). Among them, SIRT6 is a pivotal nuclear sirtuin implicated in the regulation of hepatic homeostasis and function(Zhong et al., 2020). As an important nuclear protein related to antioxidative regulation, SIRT6 safeguards hepatic damage from hepatic inflammation and oxidative stress via interplay with the nuclear factor kappa B (NF-κB) RELA subunit and deacetylates H3K9 at NF-κB target gene promoters, thus suppresses the generation of reactive oxygen species and reactive nitrogen species (ROS/RNS)(Kawahara et al., 2009; Kim et al., 2019). Recent studies demonstrate that activation of PPARα/γ could attenuate ALI through suppressing hepatic inflammation and oxidative stress(Tian et al., 2018). PPARα/γ thus are the potential therapeutic targets for the treatment of ALI, and dual PPARα/γ agonist may be a promising hepatoprotective agent. Unfortunately, until now, effective and safe dual PPARα/γ agonist in clinic is unavailable owing to serious adverse drug reactions such as tumor, cardiotoxicity and renal toxicity(Dubois, Eeckhoute, Lefebvre & Staels, 2017). Therefore, a safer and more efficacious dual PPARα/γ agonist is desperately needed. Icariside II (ICS II), a natural flavonoid compound derived from traditional Chinese medicine *Herba Epimedii*, exerts diverse pharmacological properties including anti-tumor effect(Yu, Zhou, Shi, Wang, Huang & Ren, 2022), anti-oxidant effect(Feng, Gao, Liu, Shi & Gong, 2018), anti-neuroinflammatory effect(Zheng et al., 2020), etc. During the studies, no receptors for ICS II have been identified so far. Our previous studies discover that ICS II effectively suppresses ischemic stroke-induced

neuroinflammation through up-regulation of PPARα and PPARγ protein expressions in the cortex of rats(Deng, Xiong, Yin, Liu, Shi & Gong, 2016), yet, whether PPARα/γ can serve as the receptors of ICS II to inhibit ALI-evoked peripheral inflammation and oxidative stress has remained a mystery. Although an earlier study has demonstrated that ICS II at the high dose of (50 $mg \cdot kg^{-1}$) through intraperitoneal injection causes idiosyncratic drug-induced liver injury (IDILI) *in vivo*(Wang et al., 2020), our previous study reveals that ICS II at low dose of (20 $mg \cdot kg^{-1}$) by intragastrical gavage promotes long-term neurological functional recovery after ischemic stroke in mice with a good safety profile(Gao et al., 2023). In view of the scenario mentioned above, we hypothesized that ICS II at low doses might be effective in ALI. To test this possibility, we determined the effects of ICS II on ALI induced by D-galactosamine/Lipopolysaccharide (GalN/LPS). GalN sensitizes the liver toward other stimuli, and coadministration of GalN and LPS exacerbates liver injury. Since the characteristics of the induced hepatic injury in this model is very similar to clinical characteristics of ALI, the combination of GalN/LPS to induce ALI in animal models has been extensively used to investigate the mechanisms of the pathogenesis of ALI and develop new therapeutic drugs(Kusakabe et al., 2021; Wu et al., 2018). We found that ICS II at low doses significantly reduced GalN/LPS-induced ALI in a dose-dependent manner. Mechanistic studies demonstrated that ICS II served as a natural-occurring PPARα/γ-modulating ligand to rescue ALI through inhibiting the oxidation-inflammation vicious circle *via* coactivating SIRT6. Our findings not only highlight the crucial role of PPARα/γ in ALI, but also provide ICS II as a novel potential

PPARα/γ dual agonist to combat ALI.

2. Material and methods

2.1 Animals

Specific pathogen free (SPF) C57BL/6 wild type (WT) male mice (6-8 weeks) were purchased from the Experimental Animal Center of Hunan SJA Laboratory Animal Co., Ltd., SPF 6-8 weeks old *Sirt6*-deficient (*Sirt6*$^{-/-}$) mice and littermate WT mice were obtained from the cyagen biology Co., Ltd. (Guangzhou, China). All mice were kept at 22 ℃-24 ℃ and 55%-60% humidity with a 12 h:12 h light/dark cycle and had free access to standard rodent diet and sterile water. All animal experiments *in vivo* were approved by the Ethics Committee of Zunyi Medical University, and the experimental procedures were carried out in accordance with the National Institutes of Health guide for the care and use of Laboratory animals (NIH Publications No. 8023, revised 1978).

2.2 Experimental design

Experiment 1: To determine the protective effect of ICS II on GalN/LPS-induced ALI, the C57BL/6 mice were randomly allocated into seven groups (n = 10 per group): (1) Control group, (2) ICS II 20 mg·kg^{-1} + control group, (3) GalN/LPS group, (4) ICS II 5 mg·kg^{-1} + GalN/LPS, (5) ICS II 10 mg·kg^{-1} + GalN/LPS group, (6) ICS II 20 mg·kg^{-1} + GalN/LPS group, (7) Bifendate + GalN/LPS group. Mice, except for the controls, were injected intraperitoneally with 700 mg·kg^{-1} of GalN in combination with 100 μg·kg^{-1} of LPS dissolved in phosphate-buffered saline (PBS) after being starved for 18 h. The mice were administered intragastrically different doses of ICS II (5, 10, 20

mg·kg^{-1}) once daily for 7 days before injection of GalN/LPS, and the mice of control and GalN/LPS groups received volume-matched vehicle, instead. 6 h following the GalN/LPS challenge, mice were anaesthetized with isoflurane (3.5%) for blood collection, and then immediately killed by cervical dislocation followed by removal of the liver.

Experiment 2: To investigate whether PPARα/γ are the possible therapeutic targets of ICS II on GalN/LPS-induced ALI, the C57BL/6 mice were randomly divided into five groups (n = 6 per group): (1) Control group, (2) GalN/LPS group, (3) ICS II (20 mg·kg^{-1}) + GalN/LPS group, (4) ICS II analogue + GalN/LPS group, (5) Saroglitazar + GalN/LPS group. The mice of drug-treated groups were administered with 20 mg·kg^{-1} ICS II, or ICS II analogue or 4 mg·kg^{-1} saroglitazar for 7 days before injection of GalN/LPS; and the mice of control and GalN/LPS groups received volume-matched vehicle, instead. 6 h following the GalN/LPS challenge, mice were anaesthetized and killed as mentioned above.

Experiment 3: To elucidate the role of PPARα/γ in the hepatoprotective effect of ICS II on GalN/LPS-induced ALI, mice were divided into the following six groups after CRISPR-Cas9 PPARα/γ lentivirus intravenous injection: (1) Wild type (WT)-control group, (2) WT-GalN/LPS group, (3) WT-ICS II 20 mg·kg^{-1} + GalN/LPS group, (4) PPARα/γ knock out (PPARα/γ$^{-/-}$)-control group, (5) PPARα/γ$^{-/-}$-GalN/LPS group, (6) PPARα/γ$^{-/-}$-ICS II 20 mg·kg^{-1} + GalN/LPS group. The mice were administered with ICS II (20 mg·kg^{-1}) for 7 days before injection of GalN/LPS, and the mice of control and GalN/LPS groups received volume-matched vehicle, instead. 6 h following the

GalN/LPS challenge, mice were anaesthetized and killed as mentioned above.

Experiment 4: To elucidate the vital role of Sirt6 in the hepatoprotective effect of ICS II on GalN/LPS-induced ALI by targeting PPARα/γ, the WT and *Sirt6*$^{-/-}$ mice were randomly assigned into six groups: (1) WT-control group, (2) WT-GalN/LPS group, (3) WT-ICS II 20 mg·kg^{-1} + GalN/LPS group, (4) *Sirt6*$^{-/-}$-control group, (5) *Sirt6*$^{-/-}$-GalN/LPS group, (6) *Sirt6*$^{-/-}$-ICS II 20 mg·kg^{-1} + GalN/LPS group. The mice were administered ICS II (20 mg·kg^{-1}) for 7 days before injection of GalN/LPS, and the mice of control and GalN/LPS groups received volume-matched vehicle, instead. 6 h following the GalN/LPS challenge, mice were anaesthetized and killed as mentioned above.

2.3 Survival rate and serum biochemical parameters

The survival rate of mice was monitored and recorded up to 24 h after injection of GalN/LPS. Blood was gathered from the retro-orbital vein of the eye in mice 6 h after injection of GalN/LPS. The samples were centrifuged for 10 min at 3,000 ×*g*, then the serum was collected and frozen at −20 °C. Subsequently, activities of Alanine aminotransferase (ALT) and aspartate transaminase (AST) were detected using commercially appropriate kits according to the manufacturer's protocols.

2.4 Histopathological analysis

Tissues of liver and other organs were isolated at 6 h after injection of GalN/LPS and fixed in 4% paraformaldehyde, paraffin-embedded and then cut using a microtome into 5 μm thick sections. The sections were thereafter stained with haematoxylin-eosin (H&E) for blinded histological observation. The pathological changes of organs

were assessed in randomly chosen histological fields by an optical microscope. F4/80, a marker of Kupffer cells (KCs) was analyzed by immunofluorescence (IF) microscopy, and F4/80 positive cells were quantified using Image J software.

2.5 Transmission electron microscopy (TEM)

As described in our previous study(Gao et al., 2020b), liver tissues (1 mm^3) were fixed with a 3% glutaraldehyde and 1% osmium tetroxide, then dehydrated in series acetone, infiltrated in Epox 812 for a longer, and embedded. The semithin sections were stained with methylene blue and ultrathin sections
cut with diamond knife, stained with uranyl acetate
and lead citrate. Sections were examined with JEM-1400-FLASH TEM.

2.6 Cell culture and drug treatment

Experiments *in vitro* were performed using the murine cell line KCs, which were purchased from Stem Cell Bank, Chinese Academy of Sciences. The KCs were cultured in Dulbecco's modified Eagle's medium with 100 $U{\cdot}ml^{-1}$ penicillin, 100 $\mu g{\cdot}ml^{-1}$ streptomycin and 10% fetal bovine serum in 5% CO_2 at 37 °C. The KCs were pretreated for 1 h with ICS II (1, 2, 4, 8, 16 μM) or its analogue (8 μM) or saroglitazar (10 μM), and then challenged with LPS (100 $ng{\cdot}ml^{-1}$) for 24 h.

2.7 Cell viability

Cell viability was evaluated by a cell counting kit-8 (CCK-8) assay. In brief, the KCs were treated with ICS II (1-128 μM) or ICS II analogue (1-128 μM) for 24 h. CCK-8 was added to each well and incubated at 37 °C for 2 h. The absorbance was detected using a microplate reader at 490 nm and the absorbance was utilized to measure the

cell viability. The cells cultured in control medium were considered to be 100% and the cell viability of ICS II or its analogue-treated group was represented as a percentage of the control.

2.8 Serum pro-inflammatory cytokines

Serum tumor necrosis factor (TNF)-α, IL-1β, IL-6 and IL-18 levels were detected at 6 h after GalN/LPS injection in mice or LPS stimulation for 24 h in cells with appropriate commercial enzyme-linked immunosorbent assay (ELISA) kits according to the manufacturer's protocols.

2.9 Redox status

The levels of hydrogen peroxide (H_2O_2) and lipid peroxidation (MDA), and the activities of superoxide dismutase (SOD), catalase (CAT), glutathione peroxidase (GPx) and GSH/GSSG couples were detected by appropriate commercial kits to evaluate the redox status. In brief, after treatment with drugs as mentioned above, the liver tissues or cells were washed with PBS, and then homogenized in lysis buffer. Subsequently, the lysed tissue or cells was centrifuged at 10,000 ×g for 10 min to get the supernatant. The levels of H_2O_2 and MDA, SOD, CAT, GPx and GSH/GSSG were thereafter determined using a microplate reader. Moreover, dihydroethidium (DHE) staining was utilized to evaluate endogenous superoxide anion in the liver *in vivo* as reported previously(Gao et al., 2022). Briefly, livers were collected 6 h after GalN/LPS injection and then cut into 10 μm using a cryotome. Thereafter, the samples were exposed to 5 μM DHE and placed in an incubator at 37°C for 30 min. Additionally, the mice were tail vein injected with HK Yellow-AM (100 μM), a

peroxynitrite anion ($ONOO^-$) selective probe, and imaging with small animal *in vivo* imaging system to evaluate $ONOO^-$. The fluorescent images of each group were measured at the different time interval within 1 h and the emission wavelength was set at 530 nm while the excitation wavelength was set at 480 nm.

2.10 Isolation of hepatic mitochondria

Hepatic mitochondria were isolated from hepatic tissues as previously described(Gao et al., 2023). In brief, the hepatic tissues were homogenized in appropriate medium and then centrifuged (600 ×g, 10 min). Subsequently, mitochondrial pellets were obtained after the supernatant was centrifuged at 15, 000 ×g for 5 min. Finally, the mitochondrial pellets were rinsed with appropriate medium without EDTA and centrifuged at 15, 000 ×g for 5 min.

2.11 Polarography

Mitochondrial respiration experiment was performed as previously reported(Gao et al., 2023). Briefly, hepatic mitochondria were collected from WT mice after GalN/LPS injection. A clark type oxygen electrode was used to detect the ratio of State III/State IV respiration, which is indicated the respiratory control index (RCI, an accepted measure of mitochondrial coupling).

2.12 Analysis of NADPH/$NADP^+$ ratio and ATP

The ratio of NADPH/$NADP^+$ in mitochondria was measured by a NADPH/$NADP^+$ quantification kit as previously described(Gao et al., 2020a). In brief, $NADP^+$ and NADPH levels were detected after the fractions of mitochondria were homogenized and centrifuged at 10, 000 ×g for 10 min Then the samples were heated at 60 °C for

30 min and then neutralized in the appropriate extraction buffer. The absorbance of the working solution containing glucose-6-phosphate dehydrogenase was measured according to the instruction of test kit. What's more, level of ATP in mitochondria were determined as previously described(Gao et al., 2023). Briefly, the fractions of mitochondria were collected and resuspended in appropriate buffer. Thereafter, hepatic tissues were homogenized and centrifuged with 13, 000 ×g for 10 min at 4 °C. Following, the supernatants were obtained and incubated with ATP probe, and then the absorbance was assayed using a microplate reader with 590 nm wavelength.

2.13 Western blot (WB)

The protein of liver or cell samples were obtained using a protein extraction kit and the protein concentrations were measured by the BCA protein assay kit. Then, equal amounts of protein extracts (20 μg) were fractionated with sodium dodecyl sulfate-polyacrylamide gel electrophoresis and transferred to a PVDF membrane. Subsequently, the PVDF membrane was blocked with nonfat milk (5%) in TBST for 1 h at room temperature, and then the primary antibodies were utilized: PPARα (1:1000), PPARβ (1:1000), PPARγ (1:1000), p-NF-κBp65 (1:1000), NF-κBp65 (1:1000), Ikappa B (IκB) (1:1000), SIRT6 (1:1000) and acetylated histone H3 lysine 9 (H3K9Ac) (1:1000) overnight at 4 °C. Then, species-specific HRP-conjugated secondary antibody was used to mark membrane-bound antibodies, and GAPDH (1:5000), β-actin (1:5000) or Histone H3 (1:5000) was applied as a loading control. ECL Western blot detection reagents were used to visualize representative bands and the band optical intensity was quantified by Image J software.

2.14 Quantitative reverse-transcriptase-PCR (qRT-PCR)

Total RNA was isolated with the Trizol Reagent, and utilized for complementary DNA (cDNA) with the PrimeScript RT Reagent Kit. qRT-PCR was performed with the CFX96 real time PCR detection system (Bio-Rad Laboratories Ltd, Hertfordshire, United Kingdom). The mRNA expressions were detected using specific primers: Pparα: Forward: CCTTCCCTGTGAACTGACG; Reverse: CCACAGAGCGCTAAGCTGT; Pparγ: Forward: TGAGCACTTCACAAGAAATTACC; Reverse: TGCGAGTGGTCTTCCATCAC; Sirt6: Forward: TTGGATTCCTGCAACCTGCTC; Reverse: CATGGGCTTCCTCAGCTTCC;
NF-κB: Forward: CCACCACGCTCTTCTGTCTA; Reverse: AGGGTCTGGGCCATAGAACT; Tnf-α: Forward: CTGCAAGAGACTTCCATCCAGTT; Reverse: AGGGAAGGCCGTGGTTGT; IL-1β: Forward: ATGCCACCTTTTGACAGTGATG; Reverse: CCAGGTCAAAGGTTTGGAAGC; IL-6: Forward: CAGGCCCAGAAGCATGACA; Reverse: GGCAGCCTTGTCCCTTGA; IL-18: Forward: CCTGCTCTGTCACCGATG; Reverse: CAGGGCAAAGAACAGGTCAG; Gapdh: Forward: GTATGACTCCACTCACGGCAAA; Reverse: GGTCTCGCTCCTGGAAGATG.

2.15 RNA sequencing (RNA-seq) and data analysis

Total RNA was isolated from liver tissues of mice in control, GalN/LPS, and GalN/LPS + ICS II (20 $mg \cdot kg^{-1}$) groups by Trizol buffer and then determined by an

Agilent 2100 (Agilent Technologies Co. Ltd., Palo Alto, CA, USA) analysis meter. Purification of poly-A containing RNA molecules, RNA fragmentation and strand-specific random primed cDNA library were prepared, then single-read sequencing on Illumina Nova seq 6000 were performed by the LC-Bio Co., LTD. (Hangzhou, China). Thereafter, Gene set enrichment analysis was utilized to measure the level of genes expression, and the differentially expressed genes (DEGs) were screened with fold change (FC) > 1.5 and P-value < 0.05 using R package-Ballgown for analysis of Gene Ontology (GO) functional enrichment and elucidation of KEGG pathway enrichment. Next, Venny 2.1 online tool (https://bioinfogp.cnb.csic.es/tools/venny/index.html) was used to generate Venn diagram, protein/protein interactions (PPIs) network analyses were generated using STRING 11.0 (https://string-db.org/) and displayed by Cytoscape 3.6.0 software.

2.16 In silico computational molecular docking study and *molecular dynamic (MD) simulation*

Molecular docking was applied using Autodock 4.2 software to predict the affinity of ICS II, saroglitazar or its analogue with PPARα and PPARγ. In brief, the crystal structures of PPARα (PDB code: 3VI8) and PPARγ (PDB code: 2ZK0) were obtained from the Protein Data Bank (www.pdb.org) to accomplish the in silico computational molecular docking. Then, the results were displayed by PyMOL software. Moreover, the reciprocity between PPARα/γ and SIRT6 (PDB code: 3K35) were evaluated by ZDOCK and RDOCK as reported in our previous study(Gao et al., 2020a). MD simulation was performed using Gromacs2022.3 software and the potential data was

added to the topology file of molecular dynamics system as previously described(Abraham, 2011; Van Der Spoel, Lindahl, Hess, Groenhof, Mark & Berendsen, 2005). Briefly, preprocess of small molecule was performed using AmberTools22 software and Gaussian 16W software. The free molecular dynamics simulation was carried out. The process consisted of 5000000 steps, the step length was 2fs and the total duration was 100 ns. After completed the simulation, the built-in tool of the software was used to analyze the trajectory, and the root-mean-square variance (RMSD), and root-mean-square fluctuation (RMSF). To elucidate the molecular mechanism of the compounds binding with PPARα/γ, the Abinitio Relax module encoded into the Rosetta package was used to predict 1,000 conformations of the amino acid sequences of the PPARα/γ. 100 top-ranking conformations with the lowest estimated energy was chose and the solvent-accessible surface area (SASA) in the PPARα/γ by the SASA module encoded in Gromacs 2018 package. Thereafter, the mean docking score was applied to display the binding affinity of the ICS II or saroglitazar to the PPARα/γ conformation.

2.17 Surface plasmon resonance (SPR) binding assay

Binding experiments were performed using Biacore X100 instrument (GE Healthcare, Uppsala, Sweden) with Biacore X100 and sensor chip CM5 (BR-1003-99; GE Healthcare) to verify the reciprocity between PPARα or PPARγ and ICS II. In brief, PPARα or PPARγ was dissolved in 10 mM sodium acetate (pH 5.5) and absorbed as immobilization. ICS II was diluted at 0, 4, 8, 16, 32, 64, 128, 256, 512 μM with PBS-P buffer, and SIRT6 was diluted at 0, 10, 20, 40, 80, 160, 320 nM. The time of protein

interaction was set to 120 and 300 s for dissociation. Glycine-HCl (pH 2.0, BR-1003-55; GE Healthcare) was utilized for regeneration. The Biacore evaluation 3.1 analysis software (GE Healthcare) was applied to analyze binding affinity between PPARα/γ and ICS II or SIRT6. Equilibrium dissociation constants (K_D) was determined by global fitting of the affinity data from different concentrations of ICS II or SIRT6.

2.18 Generation of PPARα/γ$^{-/-}$ mice and PPARα/γ-KO KCs

PPARα/γ$^{-/-}$ mice and *PPARα/γ*-KO KCs were produced using a CRISPR-Cas9 system. In brief, the lentivirus-based CRISPR/Cas9 KO plasmid, pHBLV-U6-gRNA-EF1-ZsGreen-T2A-BSD, with the PPARα gRNA sequences 5'-CACCGCATCTGTCCTCTCTCCCCAC-3' (forward) and 5'- AAAC GTGGGGAGAGAGGACAGATG-3' (reverse) primers; the PPARγ gRNA sequences 5'- CACCGCAACTTCGGAATCAGCTCTG-3' (forward) and 5'-AAACCAGAGCTGATTCCGAAGTTG-3' (reverse) primers. CMV drove Cas9 expression and promoter U6 drove gRNA expression. Mice were intravenous injected with with a lentiviral-packed CRISPR-Cas9 PPARα/γ (10 μL, multiplicity of infection (MOI) of 100). 28 days after lentivirus intravenous injection, the knockout of endogenous PPARα/γ using CRISPR-Cas9 PPARα/γ lentivirus was verified by Western blot, and the mice were treated with or without ICS II as mentioned above. The KCs were transfected with lentiviral-packed CRISPR-Cas9 PPARα/γ for 48 h at a 100 MOI (Hanbio Biotechnology Co., Ltd., Shanghai, China). Subsequently, the knockout of endogenous PPARα/γ using CRISPR-Cas9 PPARα/γ lentivirus was verified by Western blot. Thereafter, the transfected KCs were pretreated with ICS II

(8 μM), and then challenged by LPS for further experimental analysis.

2.19 Measurement of mitochondrial bioenergetics

Oxygen consumption rate (OCR) and extracellular acidification rate (ECAR) were measured using the Seahorse XFe96 Extracellular Flux Analyzer (Seahorse Biosciences, Copenhagen, Denmark). Briefly, the KCs were incubated in a seahorse XFe96 cell culture microplate, and pretreated for 1 h with ICS II (8 μM) and then challenged with LPS (100 $ng \cdot ml^{-1}$) for 24 h. Then the OCR was detected following sequential addition of oligomycin (2.5 μM), FCCP (1 μM), a mixture of rotenone and antimycin A (0.5 μM). ECAR was measured in media lacking glucose with the successive addition of glucose (10 mM), oligomycin (1 μM) and 2-DG (50 mM). The values of OCR and ECAR were normalized to the content of total protein per well and presented as $pmol \cdot min \cdot \mu g^{-1}$ protein and $mpH \cdot min \cdot \mu g^{-1}$ protein, respectively.

2.20 PPARα/γ activities, SIRT6 activity and NF-κB p65 DNA binding activity assay

Briefly, nuclear extracts were prepared from liver of WT or *Sirt6*$^{-/-}$ mice, and transcriptional activity of PPARα and PPARγ were assayed using the commercially available ELISA kits following the manufacturers' instructions. The SIRT6 activity was detected by a fluorimetric-SIRT6 assay kit. The NF-κB-DNA-binding activity was subsequently using electrophoretic mobility shift assay (EMSA) as previously described(Gao et al., 2023). Briefly, the NF-κB consensus oligonucleotide (5'-AGTTGAGGG GACTTTCCCAGGC-3') was labeled with biotin according to the instruction manual for EMSA. Subsequently, the signals were analyzed using electrophoresis.

2.21 Determination of ICS II in mice liver and in vitro cellular uptake by liquid chromatography-mass spectrometry (LC-MS)

Briefly, 0.3 g fresh liver tissue was homogenized with 0.3 mL saline for 300 s to obtain homogenate. 500 μL ethyl acetate were added to a 100 μL sample of homogenized liver tissue and then centrifuged (12, 000 ×g at 4 °C for 15 min). The supernatant was dried with nitrogen, and 100 μL methanol was added, vortexed mixing for 3 min, and then centrifuged (12, 000 ×g at 4 °C for 15 min). The supernatant was taken into the tube and analyzed by LC-MS (AB SCIEX). *In vitro*, the KCs were pretreated with ICS II (8 μM), and then challenged with LPS (100 $ng{\cdot}ml^{-1}$) for 24 h. The cells were washed with PBS three times and harvested with methanol. Equal number of cells were lysed by sonication and cleared by centrifugation (12, 000 ×g for 15 min at 4 °C). After the cell crushing liquid sample was dried with nitrogen, add 200 μL methanol for redissolution, centrifuge at 4 °C for 15 min at 12, 000 ×g for LC-MS analysis. ICS II (2 mg) was dissolved in methanol (10 mL) to provide the 0.2 $mg{\cdot}ml^{-1}$ ICS II standard solution. The conditions of the chromatography were as follows: Phenomenex Gemini C18100A column (150 mm× 3 mm, 3 μm); mobile phase A was 72% acetonitrile, and mobile phase B was 28% aqueous solution; temperature of column: 30 °C; and injection of volume: 2 μL. The 4000QTRAP MS procedure was carried out as follows: negative scan model with multiple reaction monitoring (MRM), and Q1: 513.2 and Q3: 366.3 for ICS II; curtain gas was set as 40 psi; ionization voltage was set as -4500 V; temperature of ion source was set as 550 °C; spray gas was set as 55 psi; and auxiliary heating gas was set as 55

psi.

2.22 Toxicity evaluation

Mice were orally administrated with ICS II (5, 10, 20 $mg \cdot kg^{-1}$) for 90 days, while the mice of control group received volume-matched vehicle. At the end of drug treatment, cardiac parameters including ejection fraction (EF), fraction shortening (FS), left ventricular end-diastolic volume (LVEDV), left ventricular end-systolic volume (LVESV), left ventricular end diastolic diameter (LVIDd) and left ventricular end-systolic diameter (LVIDs) were detected by M-mode echocardiography. Thereafter, all mice were anesthetized with isoflurane (3.5%) to collect the blood samples and organs. For hematological analysis, the blood samples were used to analyze red blood cell (RBC), red blood cell volume (HCT), hemoglobin (HGB), mean corpuscular volume (MCV), mean platelet volume (MPV), white blood cell (WBC), mean corpuscular hemoglobin (MCH), percentage of granulocytes (GRAN%), percentage of lymphocytes (LYM%), monocytes (MON), platelet (PLT), platelet pressure (PCT) by an automatic hematology analyzer (TRILOGY, Dallas, USA). To evaluate biochemical parameters, serum blood samples was centrifugated at 3000 ×g for 15 min in 4 °C, and then ALT, AST, total bilirubin (TBIL), albumin (ALB), alanine blood urea nitrogen (BUN), creatinine (CRE), glucose (GLU), total cholesterol (TC), triglyceride (TG), sodium (Na), potassium (K), and chlorine (Cl) were measured by appropriate commercial kits. The organs (lung, heart and kidney) were weighed and photographed. Organ index was calculated by the following formula: organ index (%) = organ wet weight/body weight ×100%.

2.23 Statistical analysis

The data and statistical analysis comply with the recommendations of the British Journal of Pharmacology on experimental design and analysis in pharmacology(Curtis, Ashton, Moon & Ahluwalia, 2018). All data were expressed as the means ± SEM ($n \geq 5$) and analyzed by SPSS 29.0 software. All experiments were designed to generate groups of equal size, using randomisation and blinded analysis. Statistical significance was determined using one-way analysis of variance (ANOVA) followed by Tukey's *post hoc* test or Student *t* test or two-way ANOVA followed by Bonferroni's *post hoc* test with where appropriate. All experiments were performed randomized and blinded, and $P < 0.05$ was considered statistically significant.

2.24 Materials

ICS II (purity ≥ 98%) were obtained from Shanghai Renjie Biotechnology Co., Ltd. (Shanghai, China). Epimedin A (purity ≥ 98%), an analogue of ICS II, were purchased from Solaibao Technology Co., Ltd. (Beijing, China). LPS (Escherichia coli, 0111:B4), GalN and NADPH/$NADP^+$ quantification kit were from Sigma-Aldrich (St. Louis, MO, USA). Yellow-AM, saroglitazar (purity ≥ 98%) were from MCE (NJ, USA). DHE, lipofectamine 2000, NE-PER nuclear and cytoplasmic extraction reagents were from ThermoFisher scientific (Invitrogen, Carlsbad, CA, USA). ALT, AST, TBIL, TP, ALB,BUN, CRE, GLU, TC, TG, Na, K, and Cl, TNF-α, IL-1β, IL-6, IL-18, SOD, CAT, GPx assay kits were obtained from Shanghai Renjie Bioengineering Institute (Shanghai, China). CCK-8, GSH/GSSG ratio detection assay, SIRT6 Activity Assay Kit, the primary antibodies were employed in this study,

including PPARα, PPARβ, PPARγ, SIRT6, H3K9Ac, H3, NF-κBp65, p-NF-κBp65, IκB, UCP2, GAPDH, β-actin, PPARα transcription factor assay kit, PPARγ transcription factor assay kit and NF-κBp65 transcription factor assay kit, H_2O_2 assay kit, MDA assay kit and ATP assay kit were purchased from Abcam (Cambridge, UK).

3. Results

3.1 ICS II rescues liver injury from GalN/LPS insult through PPARα/γ-SIRT6 signaling pathway

To examine the effect of ICS II on GalN/LPS-induced mortality and liver injury, we determined the survival rate of mice 24 h after GalN/LPS stimulation. The results showed that the mice began to die at 6 h and the mortality reached 80% at 24 h after injection with GalN/LPS. Whereas ICS II (5, 10 and 20 $mg \cdot kg^{-1}$) improved the survival rate in a dose-dependent manner (Figure 1a). Analysis of serum ALT and AST activities, traditional serum markers of hepatocytic damage, showed that the activities of both ALT and AST in mice treated with GalN/LPS were dramatically increased than those in the control group. However, ICS II (5, 10 and 20 $mg \cdot kg^{-1}$) significantly reduced the serum ALT and AST activities compared to the GalN/LPS group (Figure 1b, c). ICS II (5, 10 and 20 $mg \cdot kg^{-1}$) also effectively ameliorated the GalN/LPS-induced histological liver injury (Figure 1d). These results indicate that ICS II pretreatment efficiently rescues liver injury from GalN/LPS at a dose-dependent manner, and the most effective therapeutic dose was 20 $mg \cdot kg^{-1}$.

To identify the physiological pathways mediated by ICS II on GalN/LPS-induced liver injury, transcriptome analysis based on RNA-seq was executed from livers of

mice treated with GalN/LPS and GalN/LPS plus 20 mg·kg^{-1} of ICS II. A total of 3553 DEGs were identified in control *vs*. GalN/LPS groups, while 667 DEGs were identified in ICS II *vs*. GalN/LPS groups. Furthermore, 439 out of the 1106 DEGs responding to pretreatment with ICS II were associated with DEGs evoked by GalN/LPS, as reflected by Venn diagram (Figure 1e). Gene ontology analysis demonstrated that these DEGs were markedly enriched in PPAR signaling pathway, pyroptosis, oxidative phosphorylation (OXPHOS) and TNF signaling pathway (Figure 1f). There were some significant down-regulated genes identified in the study such as TNF-α, IL-1β, IL-6, IL-18, and NF-κB; there were also remarkable up-regulated genes such as PPARα, PPARγ, and SIRT6 (Figure 1g). Furthermore, PPIs in the 439 DEGs were identified after ICS II pretreatment. Among the DEGs, the circle size indicated the degree of protein linking to others. The results showed that PPARα and PPARγ were the dominant relevant signaling genes, along with other regulators including SIRT6 and NF-κB (Figure 1h). In addition, the top highly DEGs (PPARα, PPARγ and SIRT6) were validated using Western blot. Consistent with the results of hepatic transcriptome analysis, ICS II significantly increased the expressions of PPARα and PPARγ proteins after GalN/LPS stimulation (Figure 1i, j). ICS II apparently increased SIRT6 protein expression, and decreased H3K9Ac protein level following GalN/LPS (Figure 1k, l). Collectively, these findings suggest that PPARα/γ are positive modulators of Sirt6 signaling pathway, a novel mechanism proposed in safeguarding ALI from oxidative stress and inflammation. ICS II rescues ALI through PPARα/γ-SIRT6 signaling pathway.

3.2 ICS II attenuates hepatic inflammation in GalN/LPS-induced liver injury

Based on the hepatic transcriptomics data we next assessed the effects of ICS II on hepatic inflammation in GalN/LPS-induced liver injury. The results of F4/80 staining in the liver sections of mice showed that ICS II decreased the number of F4/80-positive KCs after challenged by GalN/LPS (Figure 2a, b). Moreover, ICS II also obviously increased IκB protein expression (Figure 2c), decreased NF-κBp65 phosphorylation level (Figure 2d) and NF-κBp65 activity (Figure 2e). In addition, ICS II significantly attenuated GalN/LPS-induced release of pro-inflammatory cytokines, including TNF-α, IL-6, IL-1β and IL-18 (Figure 2f-i). These findings indicate that ICS II-elicited hepatoprotective effect, at least partly, through inhibiting hepatic inflammation.

3.3 ICS II reduces hepatic oxidative stress in GalN/LPS-induced liver injury

Thereafter, we also investigate the effects of ICS II on hepatic oxidative stress in GalN/LPS-induced liver injury by determining cellular oxidative markers. The results showed that at 6 h after GalN/LPS treatment, activities of SOD, CAT, GPx and GSH (reduced)/GSSG (oxidized) couples were significantly lower following GalN/LPS stimuli than those of the control group. These decreases were rescued by ICS II in a dose-dependent manner (Figure 3a-d). Moreover, levels of H_2O_2 and MDA were significantly higher than those of the control group, while these increases were reduced by ICS II in a dose-dependent manner (Figure 3e, f). Based on the results mentioned above, 20 $mg \cdot kg^{-1}$ ICS II was selected as the optimum dose for detection of mitochondrial ROS and $ONOO^-$ level, respectively. The results showed that

GalN/LPS-treated mice had higher levels of mitochondrial ROS and RNS in the liver, as shown by DHE staining and small animal *in vivo* imaging system, whereas ICS II decreased these changes (Figure 3g-k). Moreover, there were more impaired mitochondria that were obviously swollen with damaged cristae in mice after GalN/LPS insult, whereas ICS II reversed these changes (Figure 3l, m). RCI, NADPH/$NADP^+$ ratio, ATP and protein expression of UCP2 were decreased following GalN/LPS injection, which were dramatically reversed by ICS II (Figure 3n-q). These findings suggest that ICS II effectively reduces mitochondrial oxidative stress in GalN/LPS-induced liver injury.

3.4 ICS II suppresses GalN/LPS-induced ALI *by activation of PPARα/γ*

Based on the findings mentioned above, we hypothesized that PPARα/γ might be the potential therapeutic targets of ICS II. The docking studies were used to mechanistically explore the interaction of ICS II with PPARα/γ. The docking results showed that two major interaction locations in PPARα were predicted with binding affinity of −8.37 $kcal \cdot mol^{-1}$ and −6.641 $kcal \cdot mol^{-1}$ (Figure 4a). Among the binding sites, site B is composed of ILE-339, ALA-333, TYR-334, LEU-321 and ILE-317 amino acids (Figure 4b), and site C is composed of LEU-459, THR-285, VAL-306 and LYS-292 amino acids (Figure 4c). The data of a concise distribution pattern of the docking scores showed that hydrophobic interaction plays a crucial role in the interaction of ICS II with PPARα, and hydrogen-bond interaction occurred upon LEU-331, LEU-321 and SER-280 when ICS II binding to PPARα (Figure 4d). In comparison, the predicted binding affinity and the docking scores of ICS II to PPARα

were much higher than those of saroglitazar, which is a classic dual PPARα/γ agonist (Figure 4e-h; Figure S1a). What's more, the three major interaction locations in PPARγ were predicted with binding affinity of −5.39 kcal·mol^{-1}, −5.014 kcal·mol^{-1} and −5.071 kcal·mol^{-1} (Figure 4i). Among the binding sites, site J is composed of ILE-267, ILE-341, LEU-330 and ILE-326 amino acids (Figure 4j), and site K is composed of THR-440, SER-394, LEU-436 and GLN-410 amino acids (Figure 4k), and site L is composed of LEU-468, ILE-472 and LYS-301 amino acids (Figure 4l). The data of a concise distribution pattern of the docking scores showed that hydrophobic interaction plays a crucial role in the interaction of ICS II with PPARγ. Additionally, hydrogen-bond interaction occurred upon ILE-267 when ICS II binding to PPARγ (Figure 4m). In comparison, the predicted binding affinity and the docking scores of ICS II to PPARγ were slightly higher than those of saroglitazar (Figure 4n-q; Figure S1b). Of note, the binding energies of ICS II analogue with PPARα/γ were −4.83 kcal·mol^{-1} and −2.38 kcal·mol^{-1}, which indicated that structural analog of ICS II could not bind to PPARα/γ. These findings convincingly suggest that ICS II might be a PPARα/γ-modulating ligand.

To mechanistically validate the predicted results of molecular docking, further SPR assay and *in vivo* experiments were performed. The results showed that ICS II directly bound to PPARα/γ, with an equilibrium constant of 1.876×10^{-8} M and 4.857×10^{-6} M, (Figure 4r, s). Furthermore, serum ALT and AST activities were increased following GalN/LPS insult, while ICS II at the dose of 20 mg·kg^{-1} reversed these changes. In comparison, the protective effects of ICS II on GalN/LPS-induced ALI were higher

than those of saroglitazar. In contrast, ICS II analogue did not affect these changes (Figure 4t, u). Moreover, PPARα/γ activities were decreased following GalN/LPS insult, while ICS II at the dose of 20 mg·kg^{-1} distinctly increased PPARα/γ activities. In comparison, the promotive effects of ICS II on PPARα/γ activities after GalN/LPS insult were also higher than those of saroglitazar. In contrast, ICS II analogue did not affect the PPARα/γ activities after GalN/LPS insult (Figure 4v, w). These findings verify that ICS II rescues ALI, at least partly, through directly binds to PPARα/γ and activates the PPARα/γ.

3.5 PPARα/γ deficiency counteracts the hepatoprotective effect of ICS II on GalN/LPS-induced ALI

To dissect the role of PPARα/γ in the beneficial effect of ICS II on ALI, PPARα/γ$^{-/-}$ mice were generated using the CRISPR/Cas9 system resulting in >80% loss in PPARα/γ protein expression relative to control group (Figure S2). The results showed that PPARα/γ$^{-/-}$ mice displayed more severe injury after GalN/LPS insult than that of WT mice. However, ICS II lost its hepatoprotective effect on GalN/LPS-induced ALI in PPARα/γ$^{-/-}$ mice (Figure 5a-c). We next asked whether functional PPARα/γ were required for the therapeutic outcome of ICS II on hepatic inflammation and oxidative stress. The results showed that PPARα/γ$^{-/-}$ mice showed signficantly increased inflammatory cytokines levels and NF-κBp65 activity following GalN/LPS. While the inhibitory effect of ICS II on hepatic inflammation was abrogated in PPARα/γ$^{-/-}$ mice (Figure 5d-h). Also, PPARα/γ$^{-/-}$ mice showed signficantly increased oxidative stress following GalN/LPS. Whereas the the suppressive effect of ICS II on oxidative stress

was abolished in PPARα/γ$^{-/-}$ mice (Figure 5i-o). These findings suggest that ICS II-evoked protection against ALI is, at least partly, dependent on the presence of PPARα/γ, and PPARα/γ might be a potential target of ICS II, which was in keeping with the results of molecular docking and SPR mentioned above.

3.6 ICS II restores LPS-induced mitochondrial dysfunction is dependent on PPARα/γ

Furthermore, luciferase reporter assay was performed to functionally detect the ability of ICS II to activate the PPARα/γ-driven gene transactivation *in vitro* using the mouse macrophage cell line KCs. At first, CCK-8 analysis was utilized to evaluate the safe use of ICS II. The results showed that ICS II (1–32 μM) and its analogue (1–16 μM) exerted no significant effect on the survival of KCs, however, ICS II (64–128 μM) and its analogue (32–128 μM) significantly inhibited the survival of KCs, suggesting the non-cytotoxicity of ICS II and its analogue at the concentrations of 1–32 μM and 1–16 μM (Figure S3a, b) . Therefore, ICS II and its analogue at the concentrations of 1–16 μM were used to in the following experiments. Moreover, ICS II (1–16 μM) or saroglitazar significantly reduced TNF-α, IL-1β, IL-6 and IL-18 levels (Figure S3c-f), increased PPARα/γ activities following LPS challenge in KCs (Figure S3g, h). Of note, analogue of ICS II had no effect on the activities of PPARα/γ in LPS-treated KCs (Figure S3). These findings imply that the beneficial effects of ICS II on LPS-induced injury in KCs through activating PPARα/γ.

Furthermore, in our pilot studies, PPARα/γ were KO in KCs using CRISPR-Cas9 system, which resulted in >80% loss of PPARα/γ protein expressions relative to

control cells (Figure S4). The results showed that KO of PPARα/γ increased the mRNA expressions of TNF-α, IL-1β, IL-6 and IL-18 in KCs after LPS insult, however, ICS II failed to reduce these pro-inflammatory cytokines in PPARα/γ KO KCs (Figure 6a-d). Moreover, KO of PPARα/γ increased levels of H_2O_2 and MDA, decreased the activities of SOD and CAT, and the ratio of GSH/GSSG, whereas ICS II failed to reverse these changes in PPARα/γ KO KCs after challenged by LPS (Figure 6e-i). To determine the role of PPARα/γ in the salutary effects of ICS II on mitochondrial bioenergetics following LPS challenge, mitochondrial respiration was measured using the seahorse XFe96 analyzer. The results showed that a significant decrease in the basal respiration was observed after LPS-treated group, while ICS II substantially reversed LPS-induced decrease in basal respiration. The first compound oligomycin, an ATP-synthase inhibitor, was used to detect the ATP-linked respiration. The next compound FCCP, an OXPHOS uncoupler, was added to determine the maximal respiration and assess the spare respiratory capacity. At last, rotenone and antimycin, inhibitors of complex I and III, were respectively utilized to evaluate the non-mitochondrial respiration. Similar to the basal respiration data, the ATP-linked respiration, the maximal respiration, and the spare respiratory capacity were markedly reduced in LPS-treated group. In contrast, the declines of the four phases of respiration were dramatically enhanced in the ICS II-treated cells (Figure 6j, k). What's more, ECAR was performed to explore the effect of ICS II on glucose metabolism. The results showed that ECAR was significantly elevated in LPS-treated cells, while these changes were markedly reversed by ICS II (Figure 6l, m). These

results verify the specificity of ICS II in enhancing mitochondrial bioenergetics and regulating glucose metabolism. Of note, the restorative effects of ICS II on mitochondrial respiration were lost in PPARα/γ-KO KCs (Figure 6j-m), which indicated that ICS II was dependent on the activation of PPARα/γ to rescue mitochondrial bioenergetics.

3.7 ICS II-induced activation of PPARα/γ is dependent on its interaction with SIRT6

Based on the abovementioned findings, we next explored the interaction between PPARα/γ and SIRT6. The results of molecular docking and MD simulations predicted that SIRT6 displayed strong affinity and interaction with PPARα (Figure 7a-c) and PPARγ (Figure 7d-f). Furthermore, SPR-based Biacore assay was used to evaluate the physical binding of PPARα/γ to SIRT6. The results showed that PPARα/γ bound SIRT6 with a relatively high affinity (Figure 7g, h). These findings indicate that there might exist interaction between PPARα/γ and SIRT6. Subsquently, *Sirt6* deficient mice was used to verify the role of SIRT6 in the beneficial effect of ICS II on GalN/LPS-induced ALI. The results showed that *Sirt6*$^{-/-}$ exacerbated the liver injury triggered by GalN/LPS, as evidenced by higher ALT and AST activities (Figure 7i, j) and more severe histological damage (Figure 7k), These findings confirm that SIRT6 is crucial to ICS II-evoked hepatoprotection. We then explored whether SIRT6 contributed to decreasing the hepatocellular inflammation and increasing antioxidant defense in response to ICS II-induced hepatoprotective effect. The results showed that SIRT6 deficiency resulted in an increase in TNF-α, IL-1β, IL-6, IL-18 and NF-κB

mRNA expressions in GalN/LPS-treated mice, while the inhibitory effects of ICS II on these pro-inflammatory cytokines were largely counteracted in *Sirt6*$^{-/-}$ mice (Figure 7l-p). Likewise, SIRT6 deficiency leads to an increase in superoxide dye intensity, and H_2O_2, and a decrease in SOD, CAT, GPx activities and GSH (reduced)/GSSG (oxidized) couples; however, the effects of ICS II on these oxidative stress markers were substantially abolished in *Sirt6*$^{-/-}$ mice (Figure 7q-w). These findings confirmed that Sirt6 contributed to the reduction of hepatocellular inflammation and increase of antioxidant defense in response to ICS II-induced hepatoprotection. Moreover, the results further showed that *Sirt6*$^{-/-}$ mice displayed significantly reduced PPARα and PPARγ activities in comparison to WT; while the activation of PPARα/γ by ICS II upon GalN/LPS challenge was partially abolished in *Sirt6*$^{-/-}$ mice (Figure 7x, y). These results conclusively suggest that ICS II-induced activation of PPARα/γ is, at least partly, dependent on its interaction with SIRT6.

3.8 Detection of ICS II in mice liver tissues and KCs

For validating the proposed mechanisms, we thereafter detected the presence of ICS II in liver tissues and KCs using LC-MS. The results showed that ICS II was presented in liver tissues and the content of ICS II was 0.13 mg·g^{-1} (Figure S5). In addition, ICS II also presented in cells during 24 h (Figure S6).

3.9 Toxicity of ICS II in mice

We thereafter detected the potential toxicity of long-term oral supplementation with ICS II *in vivo*. The results showed that there was no significant difference of other hematology parameters (Tab. S1), biochemical parameters (Tab. S2) and cardiac

parameters (EF, FS, LVEDV, LVESV, LVIDd and LVIDs) (Figure S7a-d) in ICS II (5, 10, 20 mg·kg^{-1})-treated groups compared to control. Moreover, the organs (lung, heart and kidney) without any histopathological changes were observed in control group and ICS II-treated groups (Figure S7e, f). These findings indicates that ICS II at the therapeutic doses is non-long-term toxic in mice.

4. Discussion

Our study unveils a new-found pharmacological property of ICS II: (1) ICS II safeguards ALI from inflammation and oxidative stress with a good safety profile. (2) ICS II directly bound to PPARα/γ, and PPARα/γ deficiency counteracts the protective properties of ICS II both *in vivo* and *in vitro*. (3) Activation of PPARα/γ contributes to the protective effect of ICS II against ALI by coactivating Sirt6. To our knowledge, this is the first report that interaction between PPARα/γ and SIRT6 contributes to the oxidative stress and inflammation in ALI, and ICS II may serve as a novel and naturally-occurring dual PPARα/γ agonist to overcome ALI.

Emerging evidence reports that ALI is accompanied by inflammation, which leads to a vicious circle where inflammation drives hepatocellular injury through accelerating generation of ROS; whereas, oxidative stress further aggravates inflammatory response and hepatic damage(Bruck et al., 2004; Rada et al., 2018). Thus, to hinder this vicious circle, efficacious agents to overcome ALI should possess remarkedly anti-inflammatory and anti-oxidative stress activities. Fortunately, we recently discovered that ICS II exerted excellent anti-neuroinflammatory and anti-oxidant properties in neurological disorders such as cerebral ischemic stroke and Alzheimer's

disease(Liu, Wang, Gao, Li, Shi & Gong, 2020; Yan et al., 2017). The above-mentioned scenario and pharmacological characteristics of ICS II prompted us to probe the therapeutic effect and its possible underlying targets of ICS II on ALI. In the present study, we clearly revealed for the first time that ICS II dose-dependently reduced lethality, decreased serum ALT and AST activities, and attenuated the histological liver injury after GalN/LPS insult. Our results clearly present a novel property of ICS II, that might have potential as a clinical agent for ALI. However, the underlying therapeutic targets of ICS II that mediate hepatoprotection is blurry. We subsequently used transcriptome analysis to predict the possible underlying mechanism of ICS II-evoked hepatoprotection on ALI. Hepatic transcriptomics pinpointed that the DEGs were mainly enriched in cellular response to inflammatory response, oxidative stress, OXPHOS, and NF-κB signaling pathways. Most importantly, there is a potential interaction between the PPARα/γ signaling molecules and the DEGs induced by ICS II. Furthermore, the results of Western blot were in agreement with transcriptomics data, and ICS II altered the protein expressions of DEGs, including PPARα, PPARγ and SIRT6. Previous studies indicates that GalN/LPS elicit the activation of KCs, the resident macrophages in liver, which can release pro-inflammatory cytokines and mediated by NF-κB signal pathway. Upon ALI stimuli, IκB, a NF-κB inhibitor, is degraded and the NF-κB-IκB complex will dissociate, which promotes NF-κB translocation into the nucleus to stimulate target genes. As we expected, ICS II inhibited the activation of KCs induced by GalN/LPS, as reflected by decreased F4/80, the marker of KCs. Furthermore, ICS II also

effectively inhibited activation of NF-κB and eventually governing the release of the proinflammatory cytokines. What is more, the role of ICS II in hepatic oxidative stress during ALI is deciphered in a later study. Oxidative stress is defined as a disequilibrium between the production and the detoxification of ROS/RNS. At the physiological level, ROS (e.g., superoxide [$O_2^{\bullet-}$]) and RNS (e.g., nitric oxide [$NO^{\bullet}$]) serve as signal molecules that modulate multiple biological responses. Conversely, excessive ROS/RNS, a consequence of dysregulated redox homeostasis, is a hallmark of ALI(Ushio-Fukai, Ash, Nagarkoti, Belin de Chantemele, Fulton & Fukai, 2021). $O_2^{\bullet-}$ is produced in mitochondria, and it is converted by SOD to H_2O_2, which, in turn, is reduced to water via the actions of CAT and the GPx/GSH system, which can degrade H_2O_2 to water and molecular O_2. $NO^{\bullet}$ can be rapidly inactivated via a reaction with $O_2^{\bullet-}$, which leads to the formation of a strong oxidant, $ONOO^-$(Pietraforte et al., 2014). Thus, mitochondria are the center of ROS/RNS generation, which impulse redox-sensitive events, and respond to ROS/RNS-mediated cellular redox state(Jia, Xu, Zhu, Liu, Zeng & Li, 2022). Mitochondrial OXPHOS defects and ROS/RNS production are ultimately attributed to mitochondrial dysfunction and hepatic death(Kanemoto et al., 2019). Of note, recent evidence highlights that tight modulation of glycolysis and OXPHOS that mediates mitochondrial biogenesis could fine-tune ROS/RNS levels, and the orchestration of mitochondrial OXPHOS and glycolysis plays essential roles during ALI(Lee, Kang, Kim, Ahn, Kim & Lee, 2017). In this study, we discovered that ICS II significantly decreased the ROS/RNS generation and elevated the antioxidant enzymes activities following stimulation of

LPS in KCs. Furthermore, LPS-induced enhancement of hepatic glycolysis and inhibition of mitochondrial OXPHOS were rescued by ICS II. These findings reveal that ICS II promotes a metabolic switch from hepatic glycolysis to mitochondrial OXPHOS, which could offer macrophagocyte with sufficient energy for ROS/RNS clearance.

Intriguingly, PPARα/γ are highly enriched in macrophages, and activation of PPARα/γ corrects abnormal glycolysis and preserves the mitochondrial OXPHOS, thereby suppressing the production of ROS/RNS and release of pro-inflammatory cytokines(Christofides, Konstantinidou, Jani & Boussiotis, 2021). Our previous study has found that ICS II up-regulated PPARα/γ protein expressions in the brain(Deng, Xiong, Yin, Liu, Shi & Gong, 2016), however whether it also exerts similar effects on PPARα/γ in response to peripheral inflammation is not clear. In addition, until now, whether ICS II can directly bind to any receptor or transcription factor in cells remains still obscure. In the present study, we found that ICS II induced the activation of PPARα/γ, but not PPARβ. We therefore examined whether ICS II can serve as a ligand of PPARα/γ. Strikingly, ICS II docked very well in the interface of PPARα/γ. while our in silico analysis and SPR assay uncovered that the structural homolog of ICS II displayed very weak interactions with PPARα/γ, suggesting that compared with other structural homolog, ICS II displays a stronger affinity toward the PPARα/γ. Strikingly, the protective effects of ICS II on ALI were higher than saroglitazar, a positive PPARα/γ dual agonist, due to ICS II has a stronger property to increase PPARα/γ activities than saroglitazar. Most importantly, PPARα/γ deficiency

counteracted the hepatoprotective effect of ICS II on GalN/LPS-induced ALI in mice. These findings validated our hypothesis that ICS II acts as a novel and natural-occurring PPARα/γ-modulating ligand to rescue ALI.

Mechanistically, LPS is known to activate specialized macrophage KCs located in the liver and induces hepatic inflammation through secretion of pro-inflammatory cytokines during ALI(Yokoyama et al., 2004). To verify the role of PPARα/γ in the beneficial effect of ICS II on mitochondrial OXPHOS in ALI, we thereafter used KCs with LPS exposure to mimic ALI *in vitro*. To correlate our *in vivo* observations with what happens *in vitro* and to gain further insight into the inhibitory mechanisms involved in the *in vitro* model of ALI arrest by ICS II or saroglitazar, a positive PPARα/γ dual agonist(Jain et al., 2018), and lentivirus specific knockout of PPARα/γ in KCs were utilized. Our findings showed that ICS II and saroglitazar significantly inhibited LPS-induced inflammation and oxidative stress in WT, but not in PPARα/γ deficiency KCs. Interestingly, consistent with the results of molecular docking and the results in *in vivo*, the structural homolog of ICS II did not exert beneficial effect on KCs challenged by LPS. As we expected, ICS II failed to preserve the mitochondrial biogenesis upon stimulation of LPS in the absence of PPARα/γ of KCs. However, any modeling for the molecular interaction of ICS II with receptors of other proteins in liver cell and/or circulating macrophages lacks physiological value after gastric administration. For validating our proposed mechanisms, we thereafter validated the presence of ICS II in liver tissues and KCs using LC-MS. Encouragingly, as we expected, ICS II could reach liver tissues and cells, which better proved our proposed

mechanisms. Corroboratively, our findings reveal that ICS II may be a novel and potent PPARα/γ-modulating ligand, and induces the activation of PPARα/γ to rescue ALI.

Recent studies have reported intriguing crosstalk between PPARα/γ and SIRT6(Khan et al., 2021; Naiman et al., 2019). Nevertheless, whether the PPARα/γ and SIRT6 axis participates in ALI, and if so, whether ICS II confers the hepatic protection on ALI requiring the reciprocity between PPARα/γ and SIRT6 are still obscure and need to be further elucidated. To answer these questions, we firstly ascertained the interaction between PPARα/γ and SIRT6 through molecular docking and SPR assay. Furthermore, after GalN/LPS challenge, Sirt6 deficiency mice developed more severe hepatic damage with inflammation and oxidative stress than WT mice. While the protective effect of ICS II on ALI was substantially counteracted in Sirt6 deficiency mice. Mechanistically, these findings conclusively underscore that ICS II activates PPARα/γ to overcome ALI, at least partly dependent on SIRT6.

Unfortunately, the use of dual PPARα/γ agonists has been limited or abandoned when clinical trials have showed either increased risk for cardiac dysfunction or other adverse effects that may be due to cardiac toxicity by compromising cardiac mitochondrial biogenesis and energy homeostasis(Kalliora et al., 2019). Additionally, an earlier study has demonstrated that ICS II at the dose of 50 $mg{\cdot}kg^{-1}$ through intraperitoneal injection cotreatment with 2 $mg{\cdot}kg^{-1}$ LPS causes IDILI *in vivo*(Wang et al., 2020), however, this dose of ICS II which induced IDILI far exceeds its therapeutic doses. Whether long-term oral supplementation with ICS II is safe at the

therapeutic doses in mice remains still unclear. Thus, we next focus on the potential long-term toxicity of ICS II in mice. Encouragingly, it is clear that daily oral administration of therapeutic doses of ICS II for 90 days could not alter hematopoietic parameters, which are used to evaluate pathological conditions of humans and animals due to they are sensitive to the toxic substances. Also, biochemical parameters and cardiac parameters were not changed by ICS II, which suggested that ICS II exerted no any toxic effect on liver function, renal function and cardiac function, as well as glucose and lipid metabolism. Moreover, there were no significantly changes of the histopathology in organs that provided a supportive proof for hematological and biochemical analysis. These findings suggest that unlike conventional dual PPARα/γ agonists, which cause cardiotoxicity and nephrotoxicity, ICS II protects against ALI at therapeutic dose with a good safety profile.

Notwithstanding, we provide direct evidence that ICS II serves as a novel and potent PPARα/γ-modulating ligand and rescues ALI, there are still several pending issues need to be addressed. Firstly, we will conduct large and well-designed cohort clinical trials in humans to evaluate the potential drug-gability of ICS II in the future. Secondly, whether the negative effects of typical dual PPARα/γ agonists can be efficiently reversed upon combined administration with ICS II will be investigated in-depth. Finally, whether the salutary effects of ICS II with activation of PPARα/γ occur in other disorders will be also explored in our next story.

5. Conclusion

Our findings reveal, for the first time, a new property of ICS II: rescuing ALI with

anti-inflammatory and anti-oxidative effects by targeting PPARα/γ-mediated SIRT6/NF-κB axis. It is concluded that ICS II may be a novel and non-toxic dual PPARα/γ agonist to conquer ALI.

References

Abraham MJ (2011). Performance enhancements for GROMACS nonbonded interactions on BlueGene. J Comput Chem 32: 2041-2046.

Bruck R, Aeed H, Avni Y, Shirin H, Matas Z, Shahmurov M*, et al.* (2004). Melatonin inhibits nuclear factor kappa B activation and oxidative stress and protects against thioacetamide induced liver damage in rats. J Hepatol 40: 86-93.

Chowdhury A, Nabila J, Adelusi Temitope I, & Wang S (2020). Current etiological comprehension and therapeutic targets of acetaminophen-induced hepatotoxicity. Pharmacol Res 161: 105102.

Christofides A, Konstantinidou E, Jani C, & Boussiotis VA (2021). The role of peroxisome proliferator-activated receptors (PPAR) in immune responses. Metabolism 114: 154338.

Curtis MJ, Ashton JC, Moon LDF, & Ahluwalia A (2018). Clarification of the basis for the selection of requirements for publication in the British Journal of Pharmacology. Br J Pharmacol 175: 3633-3635.

Deng Y, Xiong D, Yin C, Liu B, Shi J, & Gong Q (2016). Icariside II protects against cerebral ischemia-reperfusion injury in rats via nuclear factor-kappaB inhibition and peroxisome proliferator-activated receptor up-regulation. Neurochem Int 96: 56-61.

Dubois V, Eeckhoute J, Lefebvre P, & Staels B (2017). Distinct but complementary contributions of PPAR isotypes to energy homeostasis. J Clin Invest 127: 1202-1214.

Feng L, Gao J, Liu Y, Shi J, & Gong Q (2018). Icariside II alleviates oxygen-glucose deprivation and reoxygenation-induced PC12 cell oxidative injury by activating Nrf2/SIRT3 signaling pathway. Biomed Pharmacother 103: 9-17.

Gao J, Chen N, Li N, Xu F, Wang W, Lei Y*, et al.* (2020a). Neuroprotective Effects of Trilobatin, a Novel Naturally Occurring Sirt3 Agonist from Lithocarpus polystachyus Rehd., Mitigate Cerebral Ischemia/Reperfusion Injury: Involvement of TLR4/NF-kappaB and Nrf2/Keap-1 Signaling. Antioxid Redox Signal 33: 117-143.

Gao J, Long L, Xu F, Feng L, Liu Y, Shi J*, et al.* (2020b). Icariside II, a

phosphodiesterase 5 inhibitor, attenuates cerebral ischaemia/reperfusion injury by inhibiting glycogen synthase kinase-3beta-mediated activation of autophagy. Br J Pharmacol 177: 1434-1452.

Gao J, Ma C, Xia D, Chen N, Zhang J, Xu F*, et al.* (2023). Icariside II preconditioning evokes robust neuroprotection against ischaemic stroke, by targeting Nrf2 and the OXPHOS/NF-kappaB/ferroptosis pathway. Br J Pharmacol 180: 308-329.

Gao JM, Zhang X, Shu GT, Chen NN, Zhang JY, Xu F*, et al.* (2022). Trilobatin rescues cognitive impairment of Alzheimer's disease by targeting HMGB1 through mediating SIRT3/SOD2 signaling pathway. Acta Pharmacol Sin 43: 2482-2494.

Garate-Rascon M, Recalde M, Jimenez M, Elizalde M, Azkona M, Uriarte I*, et al.* (2021). Splicing Factor SLU7 Prevents Oxidative Stress-Mediated Hepatocyte Nuclear Factor 4alpha Degradation, Preserving Hepatic Differentiation and Protecting From Liver Damage. Hepatology 74: 2791-2807.

Gehrke N, Hovelmeyer N, Waisman A, Straub BK, Weinmann-Menke J, Worns MA*, et al.* (2018). Hepatocyte-specific deletion of IL1-RI attenuates liver injury by blocking IL-1 driven autoinflammation. J Hepatol 68: 986-995.

Jain MR, Giri SR, Bhoi B, Trivedi C, Rath A, Rathod R*, et al.* (2018). Dual PPARalpha/gamma agonist saroglitazar improves liver histopathology and biochemistry in experimental NASH models. Liver Int 38: 1084-1094.

Jia JJ, Xu G, Zhu D, Liu H, Zeng X, & Li L (2022). Advances in the Functions of Thioredoxin System in Central Nervous System Diseases. Antioxid Redox Signal 36: 425-441.

Kalliora C, Kyriazis ID, Oka SI, Lieu MJ, Yue Y, Area-Gomez E*, et al.* (2019). Dual PPARα/γ activation inhibits SIRT1-PGC1alpha axis and causes cardiac dysfunction. JCI Insight 4: e129556.

Kanemoto N, Okamoto T, Tanabe K, Shimada T, Minoshima H, Hidoh Y*, et al.* (2019). Antidiabetic and cardiovascular beneficial effects of a liver-localized mitochondrial uncoupler. Nat Commun 10: 2172.

Kawahara TL, Michishita E, Adler AS, Damian M, Berber E, Lin M*, et al.* (2009). SIRT6 links histone H3 lysine 9 deacetylation to NF-kappaB-dependent gene expression and organismal life span. Cell 136: 62-74.

Khan D, Ara T, Ravi V, Rajagopal R, Tandon H, Parvathy J*, et al.* (2021). SIRT6 transcriptionally regulates fatty acid transport by suppressing PPARgamma. Cell Rep

35: 109190.

Kim HG, Huang M, Xin Y, Zhang Y, Zhang X, Wang G*, et al.* (2019). The epigenetic regulator SIRT6 protects the liver from alcohol-induced tissue injury by reducing oxidative stress in mice. J Hepatol 71: 960-969.

Kolodziejczyk AA, Federici S, Zmora N, Mohapatra G, Dori-Bachash M, Hornstein S*, et al.* (2020). Acute liver failure is regulated by MYC- and microbiome-dependent programs. Nat Med 26: 1899-1911.

Krishna S, Cheng B, Sharma DR, Yadav S, Stempinski ES, Mamtani S*, et al.* (2021). PPAR-gamma activation enhances myelination and neurological recovery in premature rabbits with intraventricular hemorrhage. Proc Natl Acad Sci U S A 118: e2103084118.

Kusakabe J, Hata K, Miyauchi H, Tajima T, Wang Y, Tamaki I*, et al.* (2021). Complement-5 Inhibition Deters Progression of Fulminant Hepatitis to Acute Liver Failure in Murine Models. Cell Mol Gastroenterol Hepatol 11: 1351-1367.

Lee SB, Kang JW, Kim SJ, Ahn J, Kim J, & Lee SM (2017). Afzelin ameliorates D-galactosamine and lipopolysaccharide-induced fulminant hepatic failure by modulating mitochondrial quality control and dynamics. Br J Pharmacol 174: 195-209.

Liu MB, Wang W, Gao JM, Li F, Shi JS, & Gong QH (2020). Icariside II attenuates cerebral ischemia/reperfusion-induced blood-brain barrier dysfunction in rats via regulating the balance of MMP9/TIMP1. Acta Pharmacol Sin 41: 1547-1556.

Malireddi RKS, Gurung P, Kesavardhana S, Samir P, Burton A, Mummareddy H*, et al.* (2020). Innate immune priming in the absence of TAK1 drives RIPK1 kinase activity-independent pyroptosis, apoptosis, necroptosis, and inflammatory disease. J Exp Med 217: e20191644.

Naiman S, Huynh FK, Gil R, Glick Y, Shahar Y, Touitou N*, et al.* (2019). SIRT6 Promotes Hepatic Beta-Oxidation via Activation of PPARalpha. Cell Rep 29: 4127-4143 e4128.

Pietraforte D, Vona R, Marchesi A, de Jacobis IT, Villani A, Del Principe D*, et al.* (2014). Redox control of platelet functions in physiology and pathophysiology. Antioxid Redox Signal 21: 177-193.

Rada P, Pardo V, Mobasher MA, Garcia-Martinez I, Ruiz L, Gonzalez-Rodriguez A*, et al.* (2018). SIRT1 Controls Acetaminophen Hepatotoxicity by Modulating Inflammation and Oxidative Stress. Antioxid Redox Signal 28: 1187-1208.

Singh CK, Chhabra G, Ndiaye MA, Garcia-Peterson LM, Mack NJ, & Ahmad N (2018). The Role of Sirtuins in Antioxidant and Redox Signaling. Antioxid Redox Signal 28: 643-661.

Tian Y, Li Y, Li F, Zhi Q, Li F, Tang Y*, et al.* (2018). Protective effects of Coreopsis tinctoria flowers phenolic extract against D-galactosamine/lipopolysaccharide - induced acute liver injury by up-regulation of Nrf2, PPARalpha, and PPARgamma. Food Chem Toxicol 121: 404-412.

Ushio-Fukai M, Ash D, Nagarkoti S, Belin de Chantemele EJ, Fulton DJR, & Fukai T (2021). Interplay Between Reactive Oxygen/Reactive Nitrogen Species and Metabolism in Vascular Biology and Disease. Antioxid Redox Signal 34: 1319-1354.

Van Der Spoel D, Lindahl E, Hess B, Groenhof G, Mark AE, & Berendsen HJ (2005). GROMACS: fast, flexible, and free. J Comput Chem 26: 1701-1718.

Wang B, Chen D, Jiang R, Ntim M, Lu J, Xia M*, et al.* (2022). TIP60 buffers acute stress response and depressive behaviour by controlling PPARgamma-mediated transcription. Brain Behav Immun 101: 410-422.

Wang Z, Xu G, Wang H, Zhan X, Gao Y, Chen N*, et al.* (2020). Icariside , a main compound in Epimedii Folium, induces idiosyncratic hepatotoxicity by enhancing NLRP3 inflammasome activation. Acta Pharm Sin B 10: 1619-1633.

Wu J, Zhao Y, Park YK, Lee JY, Gao L, Zhao J*, et al.* (2018). Loss of PDK4 switches the hepatic NF-kappaB/TNF pathway from pro-survival to pro-apoptosis. Hepatology 68: 1111-1124.

Xu L, Yang Y, Wen Y, Jeong JM, Emontzpohl C, Atkins CL*, et al.* (2022). Hepatic recruitment of eosinophils and their protective function during acute liver injury. J Hepatol 77: 344-352.

Yan L, Deng Y, Gao J, Liu Y, Li F, Shi J*, et al.* (2017). Icariside II Effectively Reduces Spatial Learning and Memory Impairments in Alzheimer's Disease Model Mice Targeting Beta-Amyloid Production. Front Pharmacol 8: 106.

Yokoyama M, Yokoyama A, Mori S, Takahashi HK, Yoshino T, Watanabe T*, et al.* (2004). Inducible histamine protects mice from P. acnes-primed and LPS-induced hepatitis through H2-receptor stimulation. Gastroenterology 127: 892-902.

Yu R, Zhou Y, Shi S, Wang X, Huang S, & Ren Y (2022). Icariside II induces ferroptosis in renal cell carcinoma cells by regulating the miR-324-3p/GPX4 axis. Phytomedicine 102: 154182.

Zhao E, Ilyas G, Cingolani F, Choi JH, Ravenelle F, Tanaka KE*, et al.* (2017). Pentamidine blocks hepatotoxic injury in mice. Hepatology 66: 922-935.

Zheng Y, Deng Y, Gao JM, Lv C, Lang LH, Shi JS*, et al.* (2020). Icariside II inhibits lipopolysaccharide-induced inflammation and amyloid production in rat astrocytes by regulating IKK/IkappaB/NF-kappaB/BACE1 signaling pathway. Acta Pharmacol Sin 41: 154-162.

Zhong X, Huang M, Kim HG, Zhang Y, Chowdhury K, Cai W*, et al.* (2020). SIRT6 Protects Against Liver Fibrosis by Deacetylation and Suppression of SMAD3 in Hepatic Stellate Cells. Cell Mol Gastroenterol Hepatol 10: 341-364.

Zuo Y, Huang L, Enkhjargal B, Xu W, Umut O, Travis ZD*, et al.* (2019). Activation of retinoid X receptor by bexarotene attenuates neuroinflammation via PPARgamma/SIRT6/FoxO3a pathway after subarachnoid hemorrhage in rats. J Neuroinflammation 16: 47.

Figure Legends

Figure 1 ICS II rescues liver injury from GalN/LPS insult through PPARα/γ-SIRT6 signaling pathway. Mice were pretreated with ICS II (5, 10 and 20 $mg \cdot kg^{-1}$) for 7 days before GalN (700 $mg \cdot kg^{-1}$)/LPS (100 $\mu g \cdot kg^{-1}$) challenge. (a) The survival rates in mice were measured at different time points within 24 h (n = 10). (b) Serum ALT level (n = 6). (c) Serum AST level (n = 6). (d) Representative liver histological H&E staining. Magnification 100 × (upper panel), 400 × (lower panel); bar scale =100 μm, bar scale =20 μm. Transcriptome analysis of liver tissue by RNA sequencing from GalN/LPS-treated mice and GalN/LPS plus 20 $mg \cdot kg^{-1}$ of ICS II. (e) The DEGs were identified by Venn diagram. (f) Top 20 KEGG pathways were identified using Ingenuity Pathway Analysis. (g) Heatmap of DEGs. (h) PPI network was generated by GeneMANIA analysis. The respective node size presented the degree of linking in PPI network. Larger node (PPARα and PPARγ) shares more connection to others. Western blots was utilized to confirmed for the results of

transcriptome analysis. (i) Representative images of PPARα and PPARγ protein expressions (n = 5/group). (j) Quantification of PPARα and PPARγ protein expressions (n = 5/group). (k) Representative images of SIRT6 and H3K9Ac. (l) Quantification of SIRT6 and H3K9Ac (n = 5/group). Data are shown as mean ± SEM, $^{*}P < 0.05$ *vs.* control group; $^{\#}P < 0.05$ *vs.* GalN/LPS group.

Figure 2 ICS II reduced hepatic inflammation in GalN/LPS-induced ALI. Mice were pretreated with ICS II for 7 days before GalN (700 $mg \cdot kg^{-1}$)/LPS (100 $\mu g \cdot kg^{-1}$) challenge. (a) Representative images of F4/80 staining in the liver sections of mice. (b) Quantification of F4/80 positive staining KCs (n = 5/group). (c) Representative images and quantification of IκB (n = 5/group). (d) Representative images and quantification of phosphorylation of NF-κBp65 (n = 5/group). (e) Representative image of EMSA and semi-quantitative analysis of NF-κBp65 binding activity (n = 5/group). Blood was collected from mice at 6 h following GalN/ LPS injection and sera were analyzed for pro-inflammatory cytokines using ELISA. (f) TNF-α (n = 6/group). (g) IL-6 (n = 6/group). (h) IL-1β (n = 6/group). (i) IL-18 (n = 6/group). The expression of each protein was adjusted to *β*-actin or GAPDH as the loading control. Data are shown as mean ± SEM, $^{*}P < 0.05$ *vs.* control group; $^{\#}P < 0.05$ *vs.* GalN/LPS group.

Figure 3 ICS II attenuated hepatic oxidative stress in GalN/LPS-induced ALI. Mice were pretreated with ICS II for 7 days before GalN (700 $mg \cdot kg^{-1}$)/LPS (100 $\mu g \cdot kg^{-1}$) challenge. (a) SOD (n = 6/group). (b) CAT (n = 6/group). (c) GPx (n = 6/group). (d) GSH/GSSG (n = 6/group). (e) H_2O_2 (n = 6/group). (f) MDA (n =

6/group). (g) Mice hepatic staining by DHE, and (h) fluorescence analysis of mitochondrial ROS by DHE dyes (n = 6/group). Magnification 100 ×; bar scale =200 μm. (i, j) *In vivo* mapping of $ONOO^-$ deposition in ALI model mice, and (k) quantitative analysis (n = 6/group). (l) Representative TEM images of liver tissue. Bar scale = 2 μm (upper) or 1 μm (lower). (m) Quantification of mitochondria-related parameters including % Mitochondria area refers to the ratio of mitochondrial area to image area; mitochondrial/μm^2 refers to density of mitochondria; % abnormal mitochondria refers to the abnormal mitochondria ratio in livers (n = 5/group). (n) RCI (n = 6/group). (o) NADPH/$NADP^+$ ratio (n = 6/group). (p) ATP (n = 6/group). (q) Representative images and quantification of UCP2 (n = 6/group). Data are shown as mean ± SEM, $^*P < 0.05$ *vs*. control group; $^\#P < 0.05$ *vs.* GalN/LPS group.

Figure 4 ICS II suppresses GalN/LPS-induced ALI by activation of PPAR*α/γ*. Binding mode of compounds with PPARα/γ. (a) Top view of two PPARα–ICS II binding sites on the surface and the internal tunnel in PPARα. (b) Binding pocket of site B. (c) Binding pocket of site C. (d) The plot of hydrophobic SASA of PPARα exposed to solvent versus the mean docking score upon ICS II docking, and the best docking pose of PPARα–ICS II complex with the lowest binding free energies ($kcal \cdot mol^{-1}$). (e) Top view of two PPARα–saroglitazar binding sites on the surface and the internal tunnel in PPARα. (f) Binding pocket of site F. (g) Binding pocket of site G. (h) The plot of SASA of PPARα exposed to solvent versus the mean docking score upon saroglitazar docking, and the best docking pose of PPARα–saroglitazar complex with the lowest binding energy ($kcal \cdot mol^{-1}$). (i) Top view of three PPARγ–ICS II

binding sites on the surface and the internal tunnel in PPARγ. (j) Binding pocket of site J. (k) Binding pocket of site K. (l) Binding pocket of site L. (m) The plot of hydrophobic SASA of PPARγ exposed to solvent versus the mean docking score upon ICS II docking, and the best docking pose of PPARγ–ICS II complex with the lowest binding energy (kcal·mol^{-1}). (n) Top view of two PPARγ–saroglitazar binding sites on the surface and the internal tunnel in PPARγ. (o) Binding pocket of site O. (p) Binding pocket of site P. (q) The plot of SASA of PPARγ exposed to solvent versus the mean docking score upon saroglitazar docking, and the best docking pose of PPARγ–saroglitazar complex with the lowest binding energy (kcal·mol^{-1}). (r) The binding affinity of ICS II with PPARα. (s) The binding affinity of ICS II with PPARγ. Mice were pretreated with ICS II at the dose of 20 mg·kg^{-1} for 7 days before GalN (700 mg·kg^{-1})/LPS (100 μg·kg^{-1}) challenge. (t) Serum ALT level (n = 6/group). (u) Serum AST level (n = 6/group). (v) PPARα activity (n = 6/group). (w) PPARγ activity (n = 6/group). Data are shown as mean ± SEM, $^{*}P < 0.05$ *vs.* control group; $^{\#}P < 0.05$ *vs.* GalN/LPS group; $^{\dagger}P < 0.05$ *vs.* ICS II + GalN/LPS group.

Figure 5 ICS II-evoked protection against ALI was abolished in PPARα/γ$^{-/-}$ mice after GalN/LPS insult. Mice were pretreated with ICS II at the dose of 20 mg·kg^{-1} for 7 days before GalN (700 mg·kg^{-1})/LPS (100 μg·kg^{-1}) challenge. (a) Serum ALT level (n = 6/group). (b) Serum AST level (n = 6/group). (c) Representative liver histological H&E staining. Magnification 100 × (left panel), 400 × (right panel); bar scale =100 μm, bar scale =20 μm. (d) TNF-α mRNA expression (n = 6/group). (e) IL-1β mRNA expression (n = 6/group). (f) IL-6 mRNA expression (n = 6/group). (g) IL-18 mRNA

expression (n = 6/group). (h) NF-κBp65 binding activity. (i) Mice hepatic staining by DHE, and (j) fluorescence analysis of mitochondrial ROS by DHE dyes (n = 6/group). Magnification 100 ×; bar scale =200 μm. (k) H_2O_2 (n = 6/group). (l) SOD (n = 6/group). (m) CAT (n = 6/group). (n) GPx (n = 6/group). (o) GSH/GSSG ratio (n = 6/group). Data are shown as mean ± SEM, $^{*}P < 0.05$ *vs.* WT-control group; $^{\#}P < 0.05$ *vs.* WT-GalN/LPS group; $^{\dagger}P < 0.05$ *vs.* PPARα/γ$^{-/-}$-control group.

Figure 6 *PPARα/γ* deficiency abrogated the effect of ICS II on LPS-induced inflammation and oxidative stress in KCs. The WT and PPARα/γ-KO KCs were pretreated with ICS II for 1 h, and then challenged with LPS (100 ng·ml^{-1}) for 24 h. (a) TNF-α mRNA expression (n = 6/group). (b) IL-1β mRNA expression (n = 6/group). (c) IL-6 mRNA expression (n = 6/group). (d) IL-18 mRNA expression (n = 6/group). (e) H_2O_2 (n = 6/group). (f) MDA (n = 6/group). (g) SOD (n = 6/group). (h) CAT (n = 6/group). (i) GSH/GSSG ratio (n = 6/group). (j) Representative OCR profile at baseline and after the added oligomycin (2.5 μM), FCCP (1 μM), and rotenone/antimycin (0.5 μM). (k) Quantification of OCR (n = 6/group). (l) Extracellular acidification rate (ECAR). (m) Quantification of ECAR (n = 6/group). Data are shown as mean ± SEM, $^{*}P < 0.05$ *vs.* WT-control group; $^{\#}P < 0.05$ *vs.* WT-GalN/LPS group; $^{\dagger}P < 0.05$ *vs.* PPARα/γ$^{-/-}$-control group.

Figure 7 ICS II-induced activation of PPARα/γ is dependent on its interaction with SIRT6. (a) A reciprocity of PPARα between SIRT6. (b) The RMSD of all atoms of the PPARα between SIRT6 complex with respect to its initial structure as a function of time. (c) RMSF of residues of the whole protein in the PPARα between

SIRT6 complex during the 100 ns simulation. (d) A reciprocity of PPARγ between SIRT6. (e) The RMSD of all atoms of the PPARγ between SIRT6 complex with respect to its initial structure as a function of time. (f) RMSF of residues of the whole protein in the PPARγ between SIRT6 complex during the 100 ns simulation. (g) Binding affinity of PPARα with SIRT6 was detected by SPR assay. (h) Binding affinity of PPARγ with SIRT6 was detected by SPR assay. WT mice or *Sirt6*$^{-/-}$ mice were pretreated with 20 mg·kg^{-1} ICS II for 7 days before GalN (700 mg·kg^{-1})/LPS (100 μg·kg^{-1}) challenge. (i) Serum ALT level (n = 6/group). (j) Serum AST level (n = 6/group). (k) Representative liver histological H&E staining. Magnification 100 × (upper panel), 400 × (lower panel); bar scale =100 μm, bar scale =50 μm. (l) TNF-α mRNA expression (n = 6/group). (m) IL-1β mRNA expression (n = 6/group). (n) IL-6 mRNA expression (n = 6/group). (o) IL-18 mRNA expression (n = 6/group). (p) NF-κBp65 mRNA expression (n = 6/group). (q) DHE signal (red) showed the levels of superoxide in the liver of WT mice or WT mice. (r) DHE intensity in the liver. (s) Hepatic H_2O_2 measurements (n = 6/group). (t) SOD (n = 6/group). (u) CAT (n = 6/group). (v) GPx (n = 6/group). (w) GSH/GSSG (n = 6/group). (x) PPARα activity (n = 6/group). (y) PPARγ activity (n = 6/group). Data are shown as mean ± SEM, $^{*}P <$ 0.05 *vs.* control group; $^{\#}P < 0.05$ *vs.* GalN/LPS group, $^{\dagger}P < 0.01$ *vs.* SIRT6$^{-/-}$-control group, $^{¶}P < 0.01$ *vs.* SIRT6$^{-/-}$-GalN/LPS group.

a

PPARα binding to ICS II

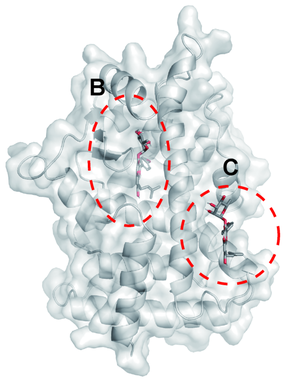

b

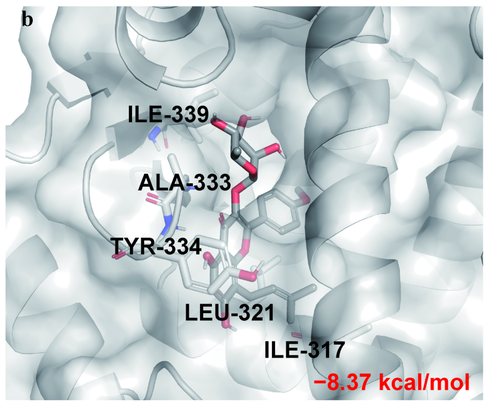

c

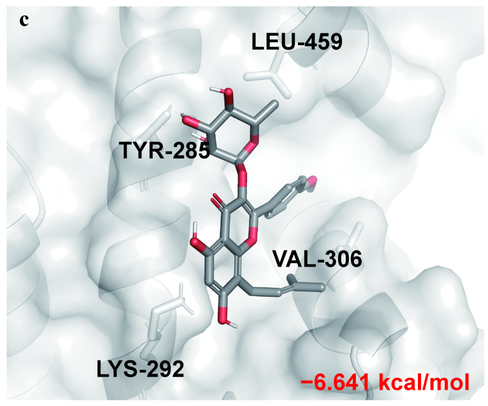

d

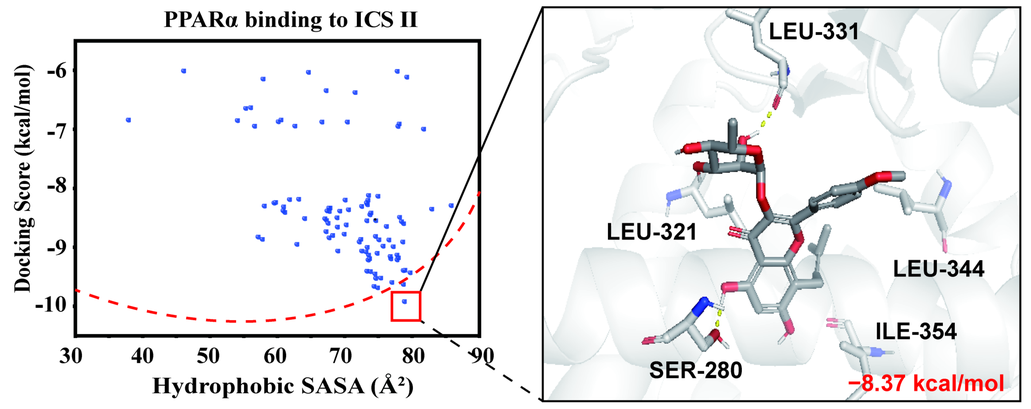

e

PPARα binding to Saroglitazar

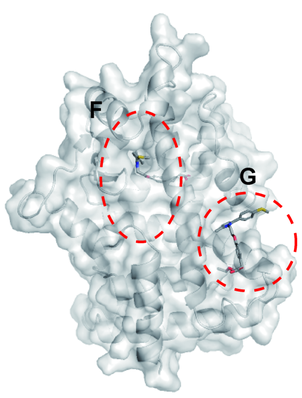

f

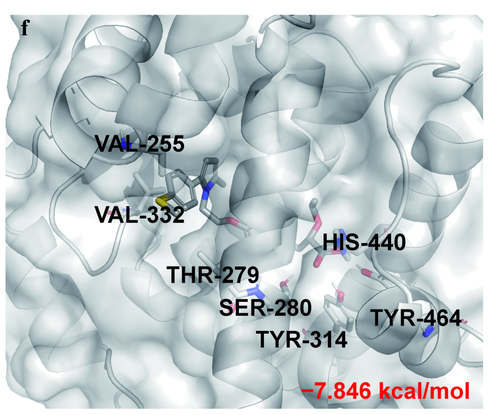

g

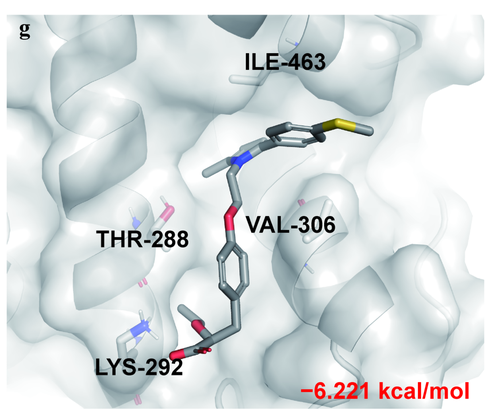

h

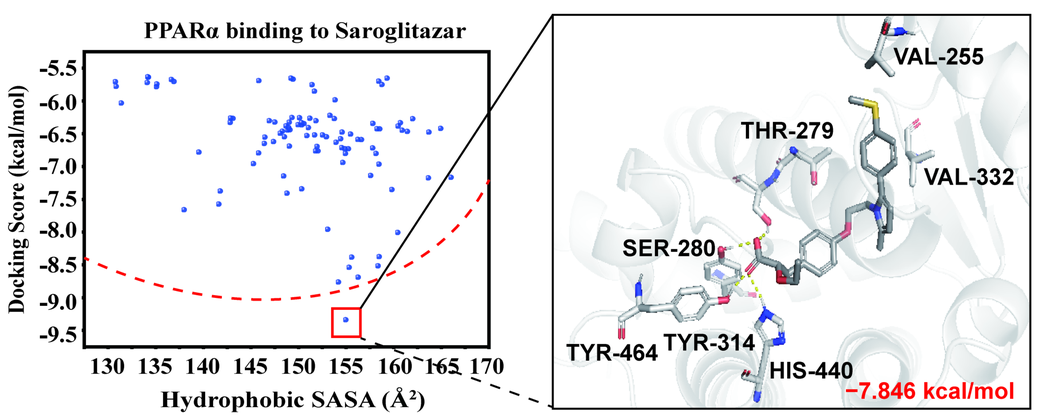

i

PPARγ binding to ICS II

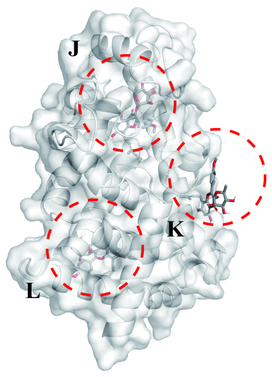

j

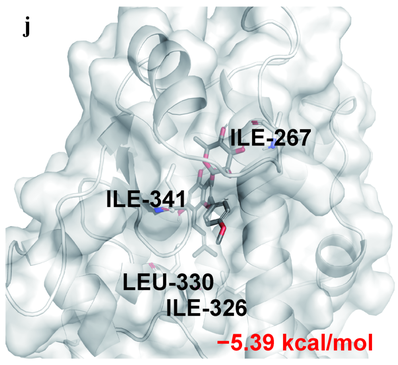

k

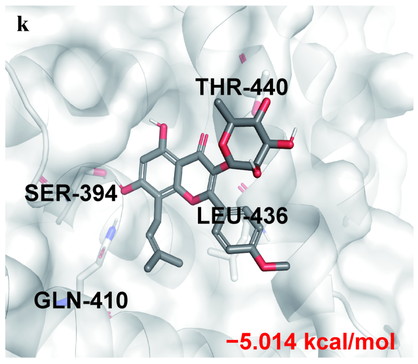

l

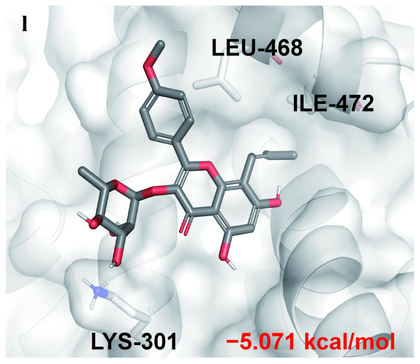

m

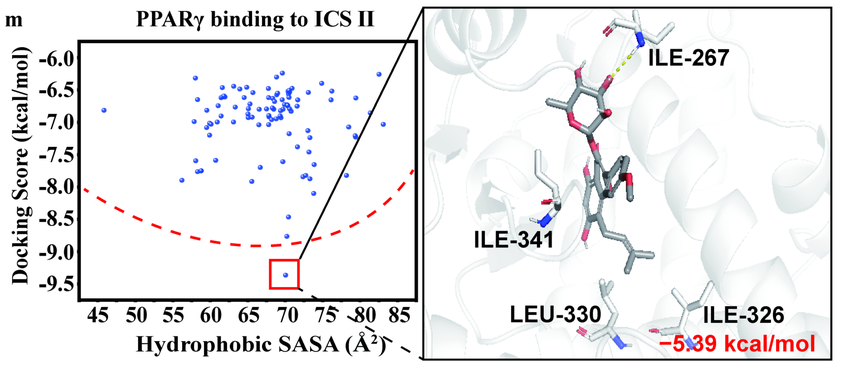

n

PPARγ binding to Saroglitazar

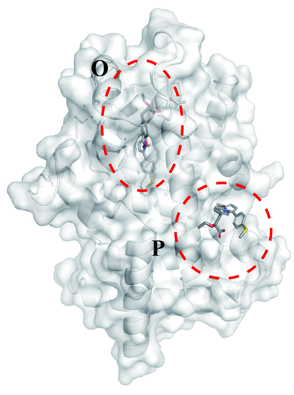

o

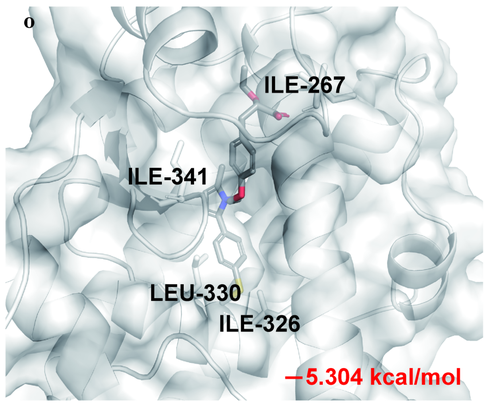

p

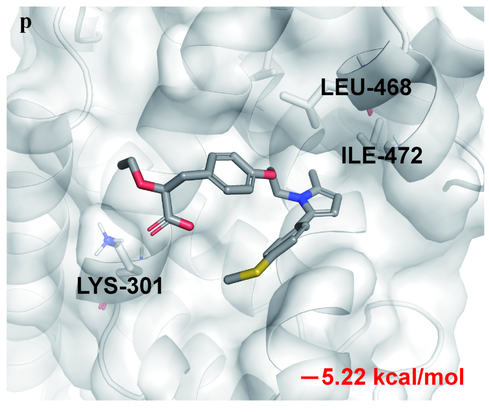

q

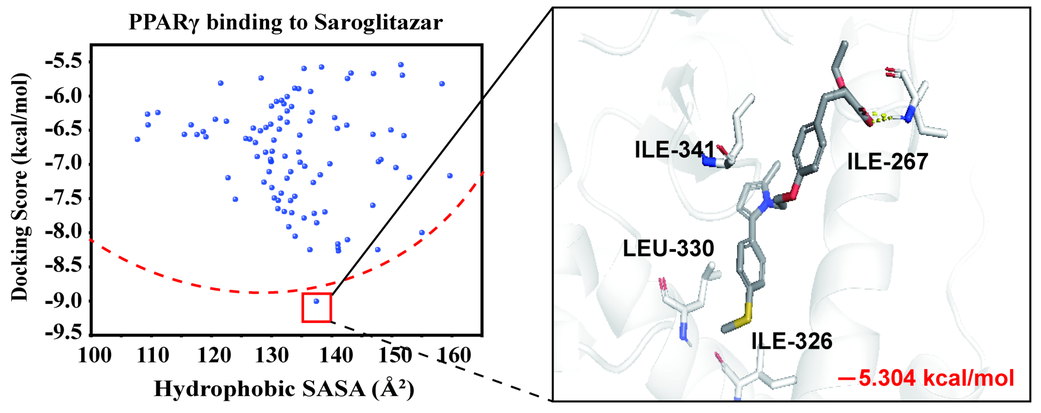

r

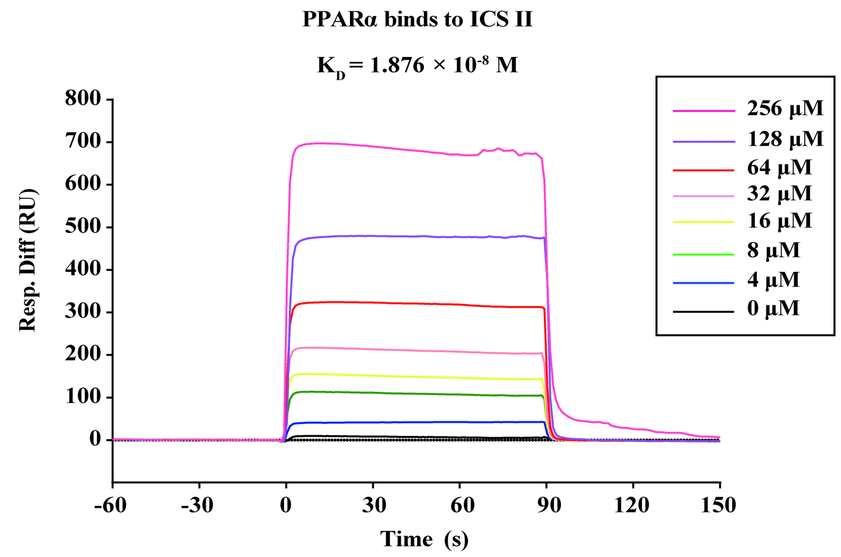

t

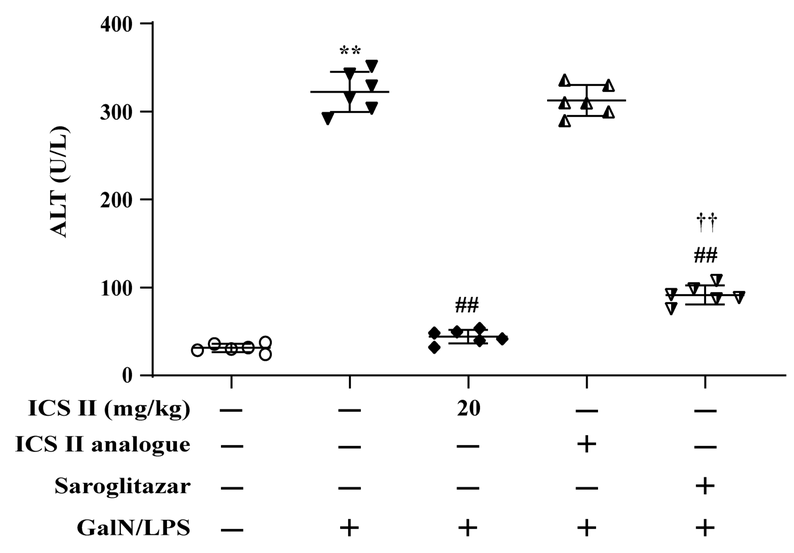

v

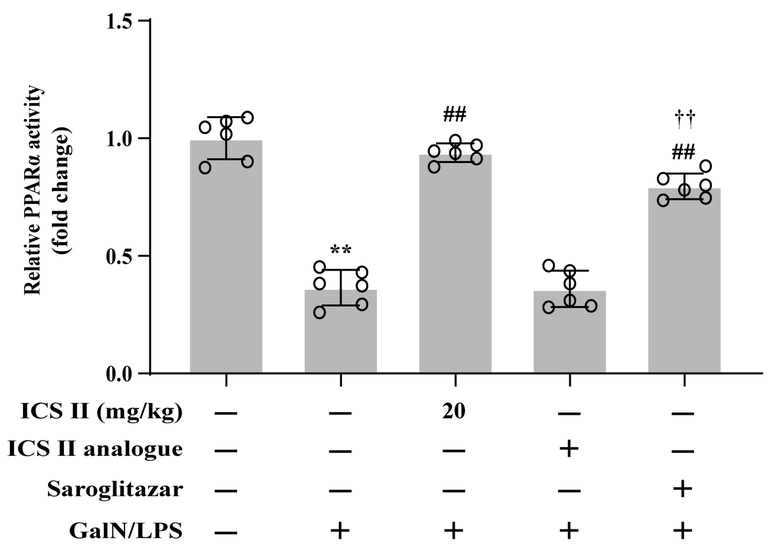

s

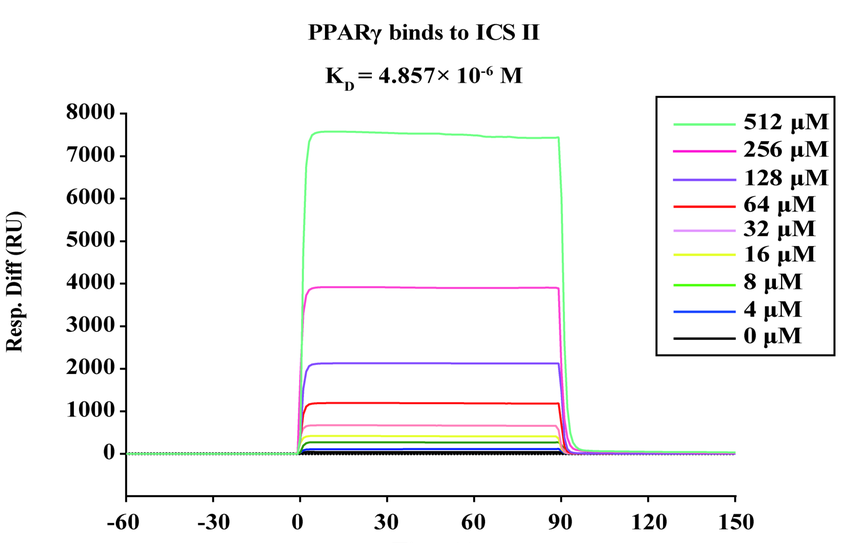

u

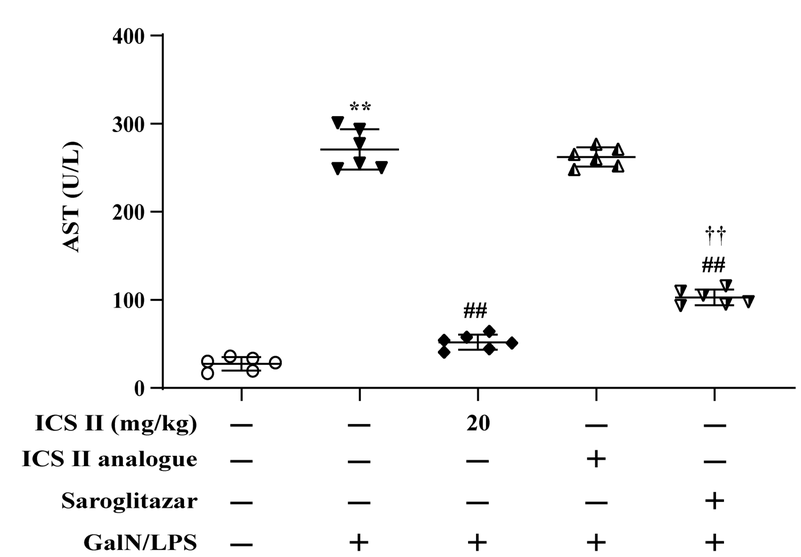

w

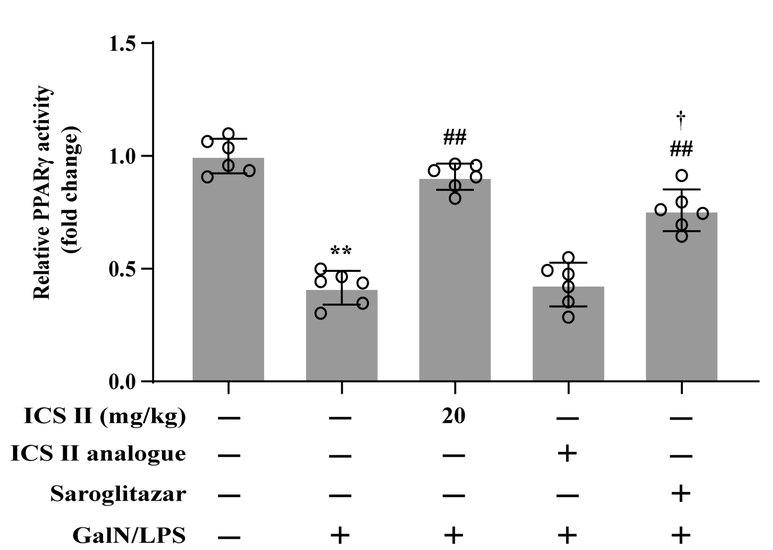

a

Docking of PPARα to SIRT6

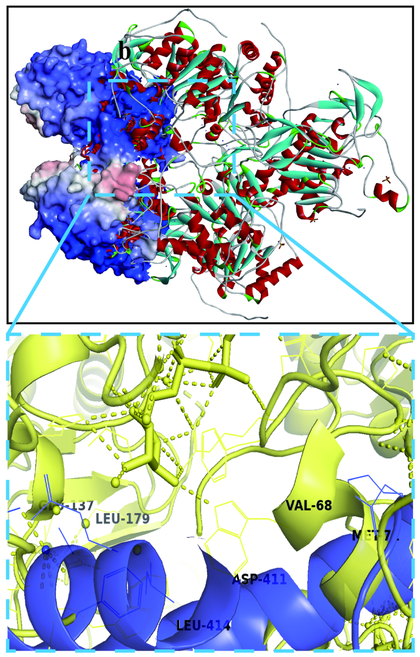

b

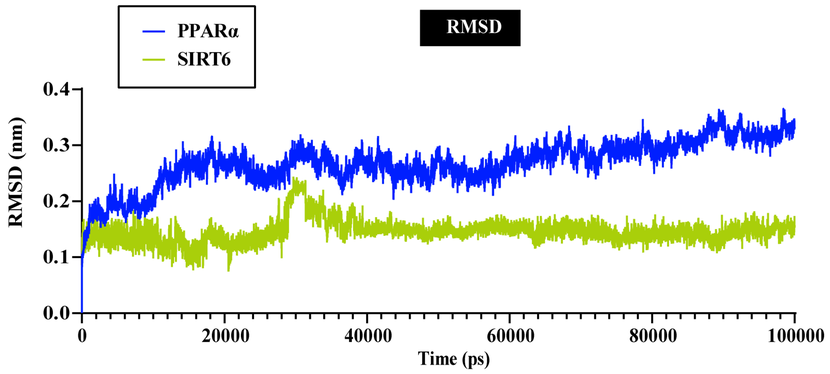

c

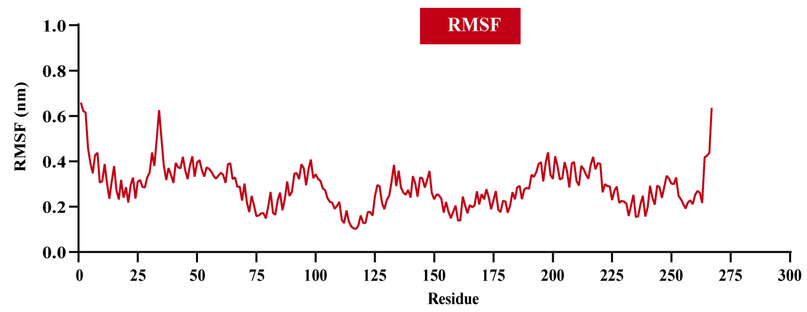

d

Docking of PPARγ to SIRT6

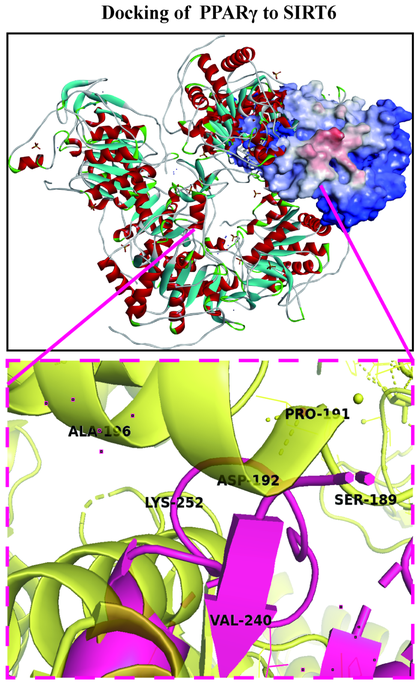

e

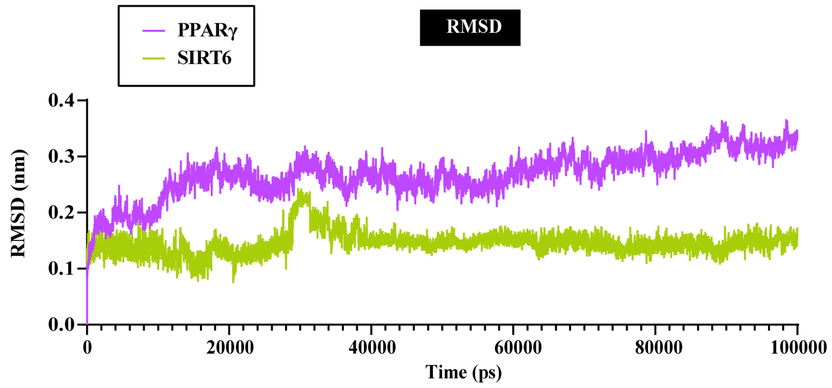

f

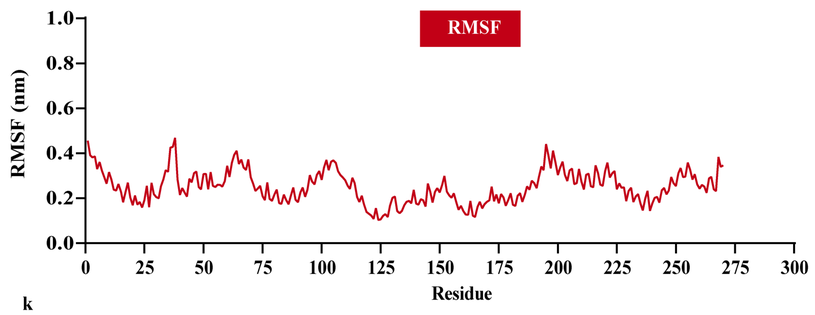

g

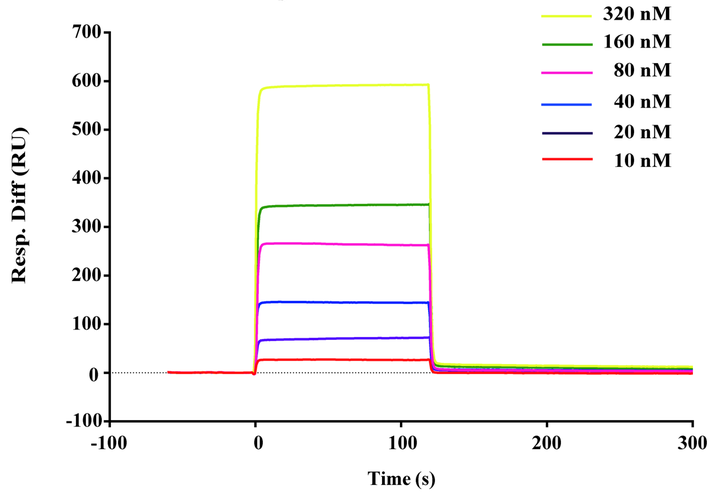

h

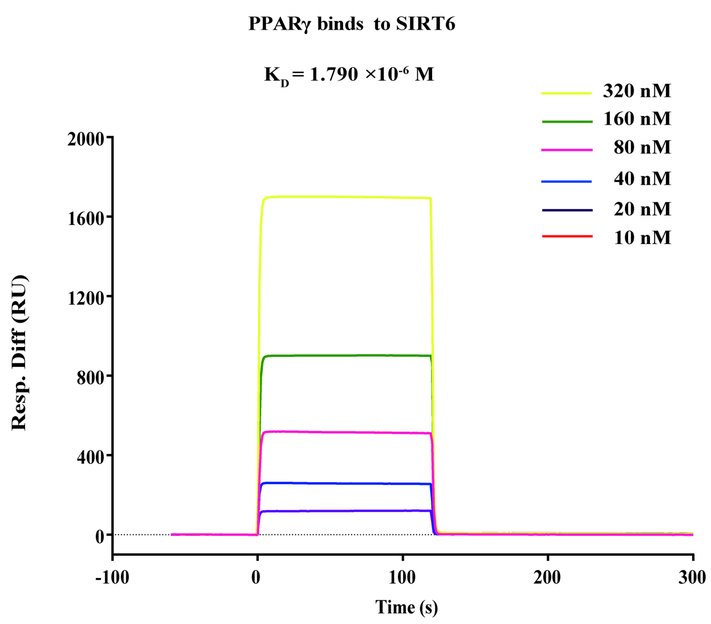

i

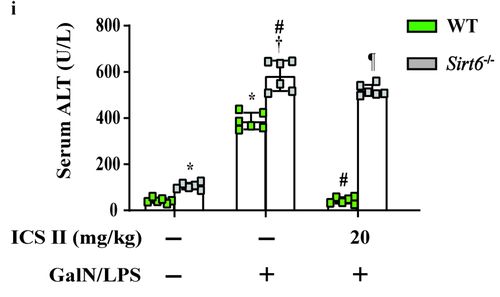

j

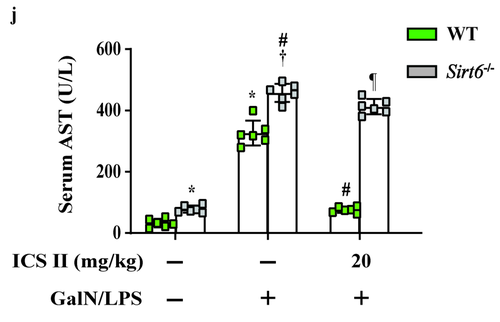

k

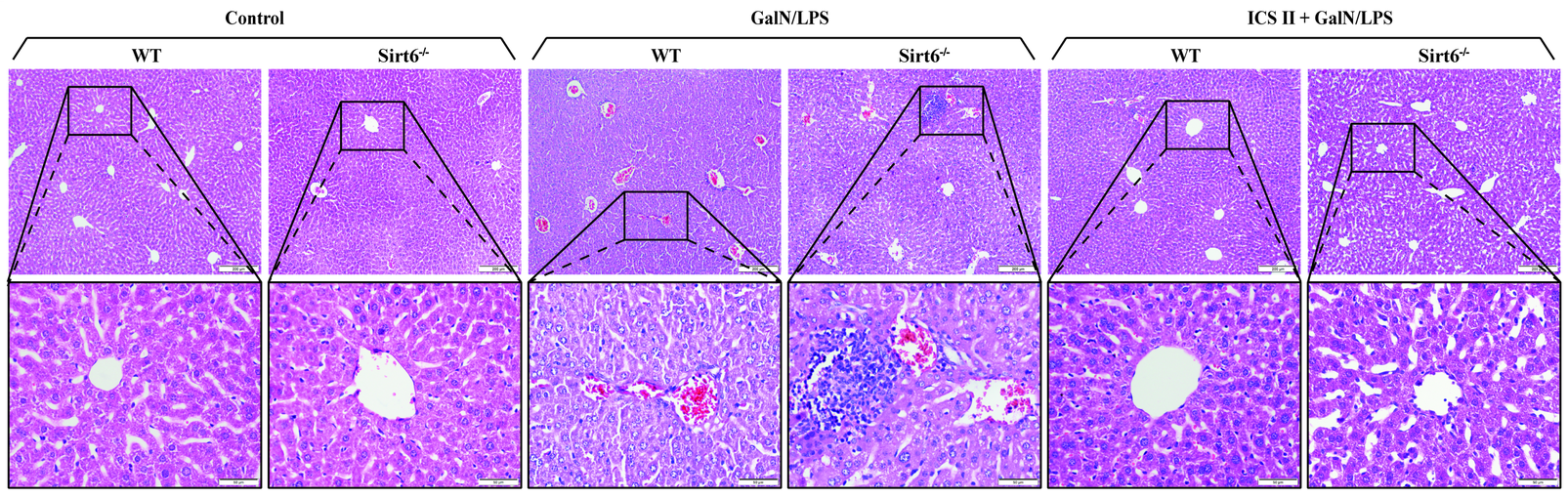

l

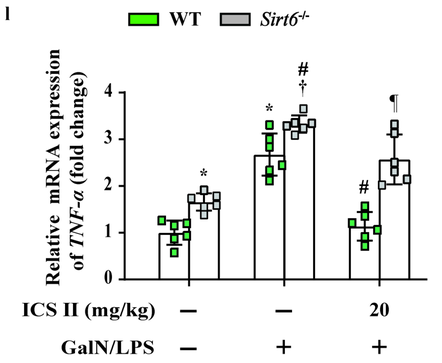

m

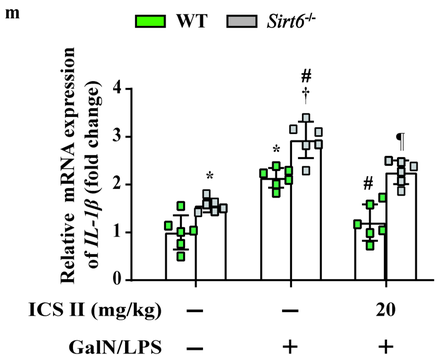

n

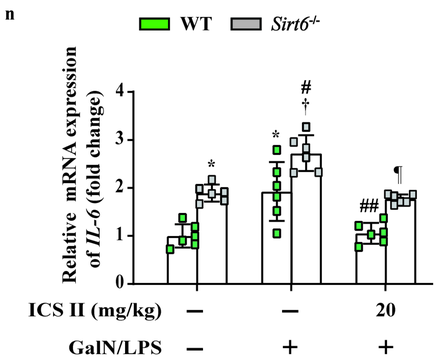

o

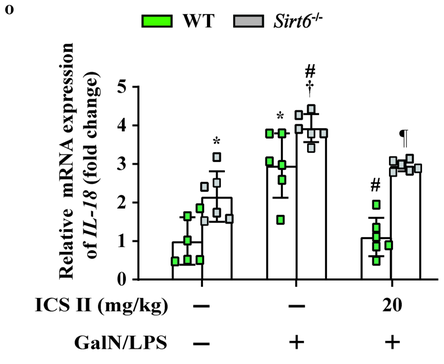

p

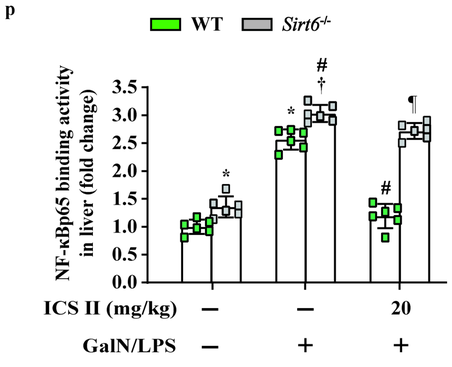

q

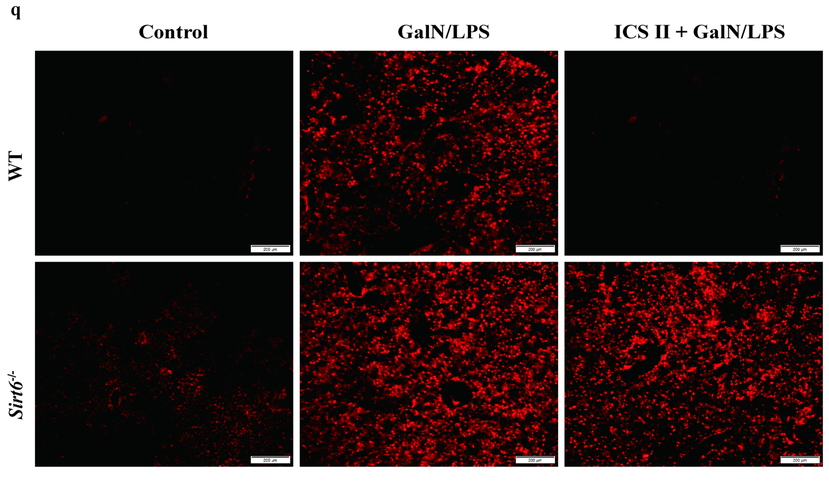

r

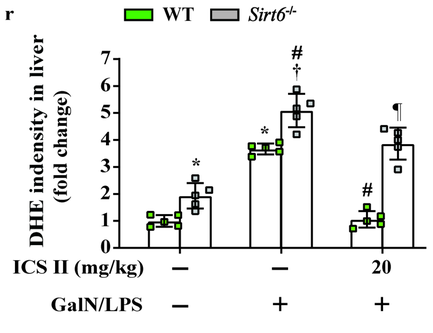

s

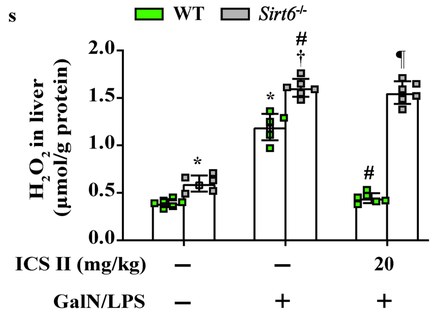

t

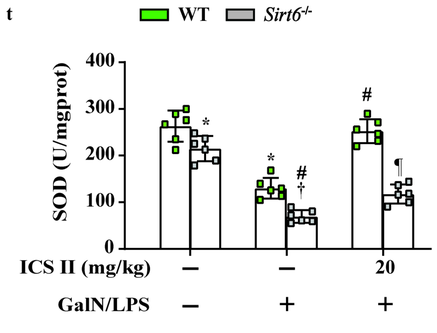

u

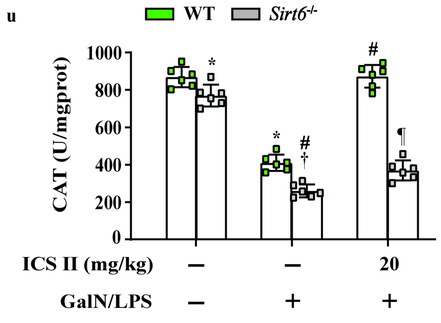

v

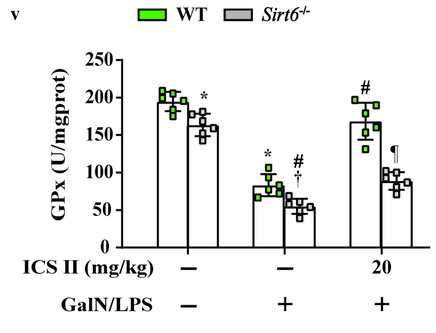

w

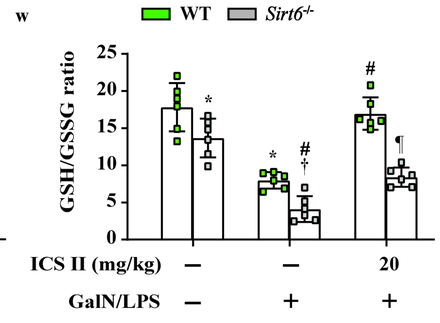

x

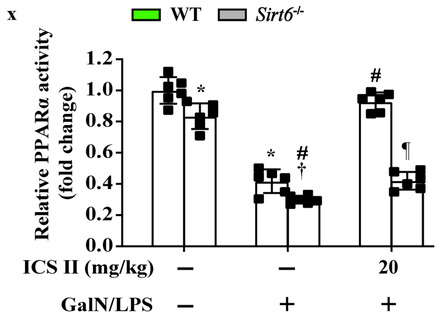

y